

A 250 GHz ESR study of *o*-terphenyl: Dynamic cage effects above T_c

Keith A. Earle, Jozef K. Moscicki,^{a)} Antonino Polimeno,^{b)} and Jack H. Freed
Baker Laboratory of Chemistry, Cornell University, Ithaca, New York 14853-1301

(Received 13 January 1997; accepted 19 March 1997)

Three nitroxide spin probes of different sizes and geometrical shape were used in a 250 GHz ESR study of the probe rotational dynamics in the fragile glass former ortho-terphenyl (OTP) over a wide temperature range from 380 to 180 K. Comparative studies at 9.5 GHz have also been performed. Perdeuterated 2,2',6,6'-tetramethyl-4-methyl aminopiperidinyl-*N*-oxide (MOTA), and 3,3'-dimethyloxazolidinyl-*N*-oxy-2',3-5 α -cholestane (CSL) are, respectively, comparable in size to and larger than the OTP host molecule, whereas Perdeuterated 2,2',6,6'-tetramethyl-4-piperidine-*N*-oxide (PDT) is substantially smaller. The sensitivity of 250 GHz ESR to the details of the rotational tumbling for $T \geq T_c$ (where T_c is the crossover temperature) was exploited to show that the relaxation is fit by a model that is characteristic of a homogeneous liquid. A nonlinear least-squares analysis shows that below the melting point, T_m , CSL, and MOTA dynamics are well-described by a model of dynamic cage relaxation proposed by Polimeno and Freed wherein the probe relaxation is significantly influenced by a fluctuating potential well created by the neighboring OTP molecules. A model of simple Brownian reorientation does not fit the experimental spectra of CSL or MOTA as well as the dynamic cage model below T_m . Spectra of PDT do not show any significant non-Brownian dynamics for this probe. It was found that the characteristic rates of the cage model, viz., the reorientation of the probe and the cage relaxation, were describable by activated processes; however, the "average" rotational diffusion rates (defined in the usual manner as the time integral of the correlation function) derived from the dynamic cage parameters follow the Stokes–Einstein–Debye (SED) relation rather well, in agreement with previous studies by other physical techniques. It is then shown that the usual stretched exponential fit to the motional correlation function, interpreted in terms of an inhomogeneous distribution of simple reorientational rates, is clearly inconsistent with the observed ESR spectrum. The absence of a significant cage potential above T_m is discussed in terms of a model of frustration limited domain sizes proposed by Kivelson and co-workers. Evidence for the existence of substantial voids in OTP below T_m , especially from the spectra of the small PDT probe, is discussed in terms of the structure and packing of the OTP solvent. © 1997 American Institute of Physics. [S0021-9606(97)51024-5]

I. INTRODUCTION

The origins of glass formation have attracted considerable and sustained experimental and theoretical attention for nearly a century. It has been well established that when various liquids, ranging from simple, single component systems to polymers, multicomponent mixtures, and colloids, are supercooled, a single relaxation process characteristic of higher temperatures bifurcates into two distinct relaxation processes: Namely a slower, primary (or α) and a faster, secondary (or β) process at some critical (or crossover) temperature T_c . Characteristically, T_c is several tens of degrees above the calorimetric glass transition temperature, T_g . The α relaxation is non-Arrhenius in character and freezes out around T_g , while the β process remains Arrhenius-like upon lowering the temperature. Viscosity measurements and dielectric spectroscopy were the primary tools for studying these relaxation processes in the past. Both these methods report on the many-body response of the system to an exter-

nal perturbation. Therefore, the concept of cooperative many-body motion has been a natural assumption in the interpretation of the behavior of supercooled liquids for more than five decades. But this has yet to lead to a complete understanding of the phenomenon.

A. Theories for the liquid to glass transition

Jenckel was probably the first to introduce the idea of many body cooperative rearrangements in regions ("Gruppen") the sizes of which are temperature dependent, to explain the non-Arrhenius behavior of viscosity upon approaching T_g .¹ This concept was explored further by Adam and Gibbs² who assumed that these "cooperatively rearranging regions" (CRR) form a subsystem of the sample which goes from one configuration to another independent of its environment. The CRR picture has been further explored by considering the existence in supercooled liquids of dynamical domains which may or may not be spatially distinct.^{3,4}

However, neither of the models was specific about the dynamics of individual molecules with respect to each other. Other investigators have explored a wide range of ideas referring to the underlying mesoscopic mechanism of the liquid to glass transition in order to explain experimental findings in supercooled liquids and especially the way a probe

^{a)}Permanent address: Smoluchowski Institute of Physics, Jagiellonian University, Reymonta 4, 30-059 Krakow, Poland; ufmoscic@cyf-kr.edu.pl

^{b)}Permanent address: Department of Physical Chemistry, University of Padova, via Loredan 2, 35131 Padua, Italy; ninop@cfalfa2.chfi.unipd.it

molecule couples to its neighbors in its dynamical behavior.

A theoretical model based on the free volume concept was introduced by Cohen and Turnbull⁵ to explain the dramatic changes in the viscosity, diffusion, and the mean (dielectric) relaxation time of the α process between T_c and T_g . The fundamental assumption of the free-volume theory is that a diffusing molecule is trapped in a cage by the surrounding molecules except for the short periods when there are substantial displacements that contribute to the overall diffusion process.^{5,6} A redistribution of the free volume within the sample will occasionally enlarge the trap, thereby enabling a displacement. The theory rationalized phenomenological Doolittle and Vogel–Fulcher–Tammann laws, often used to parametrize experimental findings from T_g to well above T_c . Although the theory does not specify a particular mechanism for the free volume redistribution, an important feature of this simple but conceptually attractive theory rests on its strong coupling of the monomolecular dynamics to the structural dynamics of the neighborhood, thereby implying a similar origin for the single molecule and many-body behavior.

The concept of heterogeneity in the supercooled system was the key idea that has carried over to other theoretical approaches to the molecular dynamics. Although two opposing concepts of how the molecular dynamics is coupled to dynamics of the local environment have been intensively explored in the past, the emerging picture remains unclear. On the one hand, is a model that assumes the existence of rigid domains in the system. It was first suggested by McLaughlin and Ubbelohde⁷ and has subsequently been explored by Stillinger⁸ and by Kirkpatrick *et al.*⁹ They have presented models of glassy state formation that results from the existence, within the otherwise fluid system, of strongly bonded domains which preserve their integrity in the course of translational and rotational motions. The concept is useful in explaining a paradoxical discrepancy between rates of translational and rotational diffusion as the supercooled liquid approaches T_g , namely a significantly weaker temperature dependence of translational diffusion compared to rotational diffusion.^{10,11}

On the other hand, this translation–rotation paradox can also be fit satisfactorily with models emphasizing the importance of system fluidity, by assuming the coexistence of fluid- and solidlike regions in the supercooled liquid, with molecular dynamic events taking place in liquid regions.^{12–16}

A recent theoretical model of Kivelson and co-workers^{17,18} emphasizes a different point of view that may be relevant in current work to unravel the approach to the glass transition. The key feature of this model is the assumption of an avoided thermodynamic phase transition at a temperature $T^* \geq T_m$. Above T^* , there is so much kinetic energy in the system that it is impossible to form long-lived domains. Below T^* , it is assumed that there is a preferred local structure within the solvent that differs substantially from the actual structure of the crystal phase. The local structure cannot be sustained over all space in the thermodynamic limit, otherwise the local structure would be the crystalline structure, contrary to the assumption of the model. Kivelson

and co-workers model the situation by postulating that the hamiltonian for the system has a term that describes the local structure plus a perturbing term that models frustration within the system and prevents the local structure from becoming a global one. It is the frustration term that prevents the phase transition at T^* . They were able to show that the model is quite successful in rationalizing bulk properties such as the shear viscosity and the temperature dependence of the average relaxation time for the α process in a variety of strong and fragile glass formers¹⁸ over a broad range of temperatures. As the model stands, it is limited to a description of the α relaxation process. Nevertheless, the theory makes predictions about the behavior of glass formers on a microscopic level in the range between T_m and T_c , and it is an important experimental problem to test whether the assumptions of the frustration limited domain model are valid or not.

The mode-coupling theory of the glass transition^{19–22} (MCT) attempts to elucidate the α and β processes in supercooled liquids and is, in that sense, a more general theory than the frustration limited domain model of Kivelson and co-workers. MCT stipulates that as a result of nonlinear interaction effects between density fluctuations, there is dynamical feedback which leads to a sharp crossover of dynamics from fluidlike to solidlike on increasing the coupling constants towards a certain critical value, e.g., by lowering the temperature of the system or upon increasing the system density towards critical values T_c and ρ_c , respectively. On approaching this ergodic to nonergodic transition point two structural relaxation processes are predicted. The slower, α_{MCT} process freezes out at the transition, but the faster, β_{MCT} process associated with the localized motion survives into the glass phase.

As successful as MCT has been at explaining some important, universal features of the experiments at the glass transition,^{23–28} the physical nature of the modes that are coupled is unclear and this makes molecular details of the phenomena difficult to identify. In fact, MCT cannot yet provide answers to many intriguing and important questions related to quantitative differences between different materials. This includes not only a variety of possible universal complex relaxations but also the details of molecular dynamics of the glass forming liquids. Undoubtedly, further progress in the matter requires a better characterization of the molecular dynamics of complex liquids.

B. ESR experiments at high frequencies

As this brief review of theoretical models illustrates, an experimental technique sensitive to details of the molecular dynamics in the supercooled region is timely and important for elucidating the role of structural heterogeneity, complex dynamics, and cooperative behavior in supercooled liquids. It has been shown over the years that the electron spin resonance (ESR) spectra of nitroxide spin probes in liquids, although they arise from individual spin-bearing molecules, are very sensitive to a range of interactions between the spin–probe and its surroundings, and this yields much useful

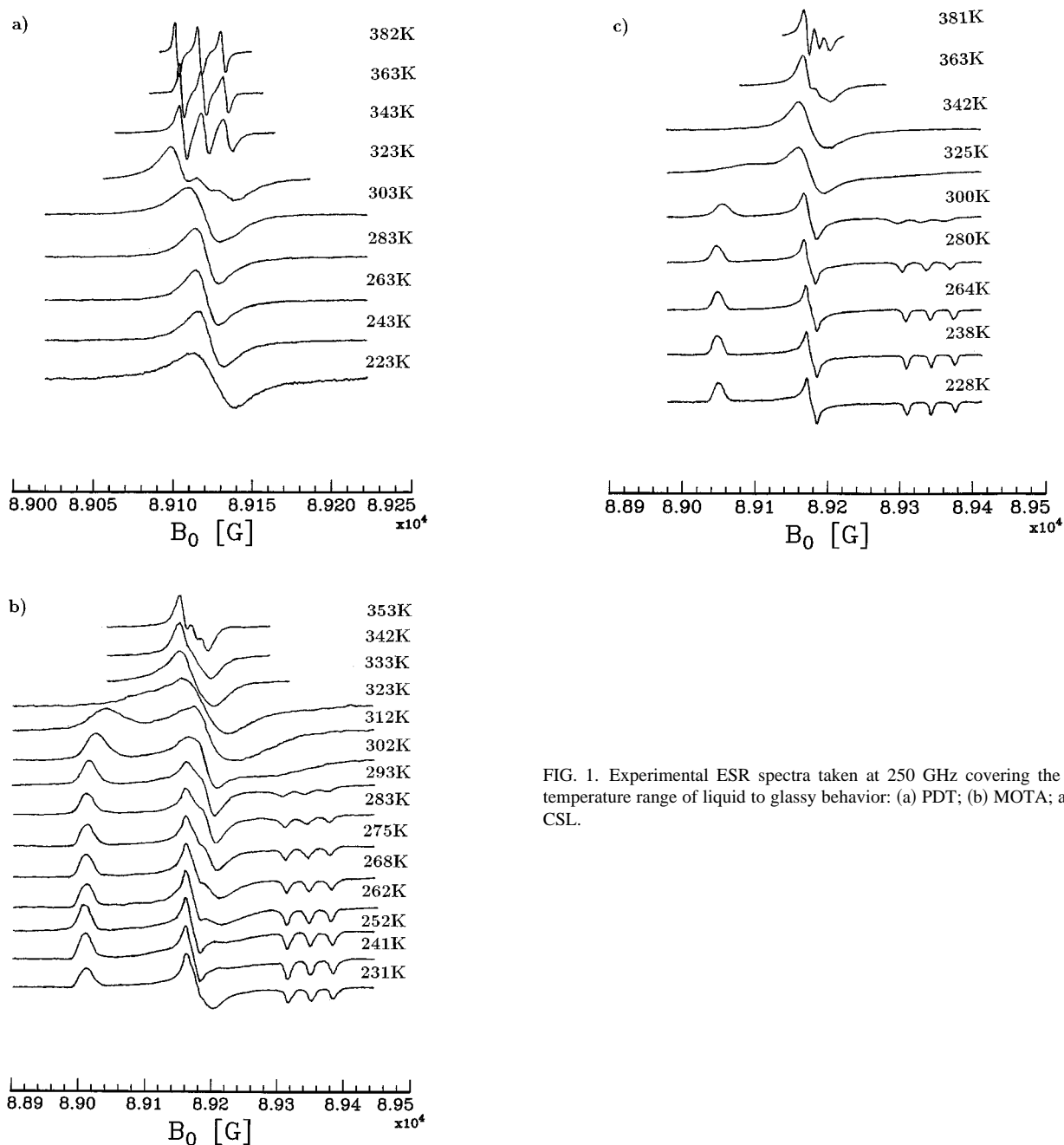


FIG. 1. Experimental ESR spectra taken at 250 GHz covering the entire temperature range of liquid to glassy behavior: (a) PDT; (b) MOTA; and (c) CSL.

insight into the spin probe dynamics in the host liquid. This is very well illustrated by results from the present study, see Fig. 1. At the highest temperatures studied, probe rotational rates are fast enough that the complex details of the spectral lines are averaged out to give simple Lorentzians. This is commonly referred to as the “fast motional regime” (fmr). Because of this averaging, only estimates of rotational rates, but not dynamic details, can be determined in this regime. As the molecular dynamics slows down upon cooling, the spectrum becomes more sensitive to the microscopic details of the motional processes involved, cf. the $280 < T < 360$ K spectra in Figs. 1(b) and 1(c). This is known as the “slow motional regime” (smr), and it constitutes the most desired experimental condition. On further slowing down of the ro-

tational dynamics, the spectrum loses its sensitivity to the dynamics. This is the so-called “rigid limit regime” (rl), cf. Figs. 1(b) and 1(c). Note that the spectra shown in Fig. 1 are all obtained at an ESR frequency of 250 GHz and 9 T magnetic fields.²⁹ At these high frequencies the ESR spectra of spin-probes in liquids are more commonly found in the smr²⁹ than is the case at a conventional ESR frequency of 9.5 GHz, (cf. Fig. 2). Another important feature of very high frequency ESR in the smr is the enhanced orientational selectivity, which is largely due to the greatly enhanced \hat{g} tensor resolution. This provides improved sensitivity to the details of microscopic features of rotational motions.

ESR studies in the smr necessitated the development of theories accounting for microscopic details of the rotational

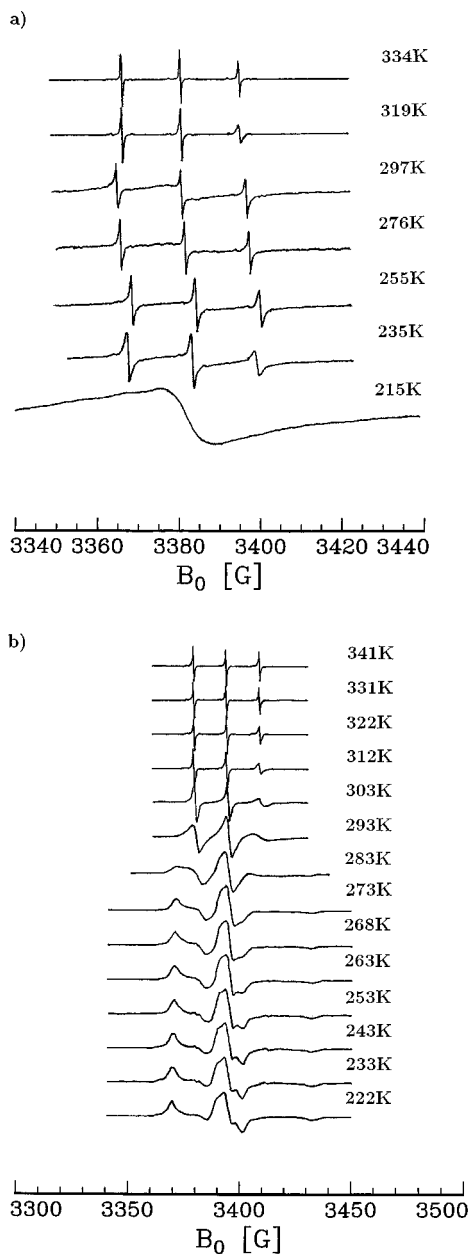


FIG. 2. Experimental ESR spectra taken at 9.5 GHz covering the entire temperature range of liquid to glassy behavior: (a) PDT; (b) MOTA.

molecular motions beyond simple relaxation theories.^{30,31} It is commonly assumed that in liquids each constituent molecule feels the effects of a cage formed by its nearest neighbors. Recently we have developed a model of the smr ESR spectrum for a nitroxide spin probe reorienting within a dynamic orientational potential well (i.e., the “dynamic cage”; both terms are synonymous in the following).³² This model has been utilized satisfactorily in analyzing two-dimensional Fourier-transform ESR spectra of spin probes in a liquid crystal.³³ As we show in this paper, this theory can be also applied to the analysis of ESR spectra in a glass-forming solvent to successfully infer the dynamics of the probe and of the host solvent cage.

We studied three different nitroxide spin-probes dis-

solved in *ortho*-terphenyl (OTP), a nonpolar organic liquid, which is one of the most extensively studied “model” glass forming systems^{34–38} (cf. also the references given in these papers). OTP has a weak tendency to crystallize, with a convenient melting point,³⁹ $T_m \approx 332$ K and a glass (calorimetric) temperature,³⁷ $T_g \approx 243$ K. According to Angell’s nomenclature⁴⁰ OTP is a fragile glass former. The crossover temperature for OTP, T_c is found to be about 50 K above T_g . The nearly nonpolar character of OTP (dipole moment,⁴¹ $\mu_D = 0.24$ D), as well as the fact that it is an unassociated van der Waals liquid, means that it has well-defined rigid molecular units weakly linked by nondirectional interactions. For all of these reasons, OTP is an excellent model system to study the glass transition and the approach to the glass transition without the complications of network structures or intertwined chain segments.³⁴ The quantitative analysis of the ESR spectra in this work focuses on results from the temperature range above T_c , where the spectra of all three spin-probes are most sensitive to the details of motion.

Our experimental results obtained indicate that the dynamic cage is not manifest in the probe rotational dynamics above T_m . The story changes significantly below T_m where the cage orientational potential plays an important role in the dynamics of the spin-probes, and it has a natural interpretation in terms of the growth of frustration limited domains, as we argue below. The cage potential is also characteristic for each spin-probe as we discuss below. An interesting result that emerges from our analysis is that the underlying cage relaxation rate is the same (to within experimental error) for all our spin-probes, which gives us confidence that the spin-probes are truly reporting on dynamical processes within the supercooled OTP.

We also show that, whereas our cage and probe relaxation rates have simple Arrhenius behavior, the average relaxation rate shows non-Arrhenius behavior, consistent with the results from other spectroscopies such as NMR^{23,37} and dynamic light scattering.^{11,42} We then show that the interpretation in terms of heterogeneous distributions of independently relaxing domains⁴³ is inconsistent with the observed experimental ESR spectra and that the relaxation in the range $T > T_c$ is homogeneous within our resolution, but described by complex dynamics.

This paper is organized as follows. The experimental methods and measurements are described in Sec. II. We present the general observations and results in Sec. III. Since the spectral simulations and least-squares fitting to experiment constitutes an integral part of the work, it is also included in this section. Discussion of our results (Sec. IV) and a summary of our findings (Sec. V) follow.

II. EXPERIMENT

As discussed in the previous section, the best sensitivity of ESR spectra to the microscopic details of the motional process occurs in the slow motional regime. This smr corresponds to the limit $\Delta\omega \gg R$, where R is the rotational rate of the probe and $\Delta\omega$ is a measure of the magnitude of the orientation-dependent part of the spin Hamiltonian. The lat-

ter is a function of properties inherent to a given spin-probe, i.e., the \hat{g} and hyperfine tensors,⁴⁴ and of the static magnetic field.

Because of the high rotational rates characteristic of the molecular dynamics of tracers in typical liquids at ambient temperatures, smr spectra are not frequently observed at conventional frequencies e.g., 9.5 GHz, but this situation changes significantly if one goes to high microwave frequencies, e.g., 250 GHz, where $\Delta\omega$ becomes significantly greater, due to the enhanced role of the \hat{g} tensor.

The main experiments of the present study were therefore performed on a home-built 250 GHz EPR spectrometer,^{45,46} with additional experiments on a commercial Bruker X-band spectrometer. The ability to observe 250 and 9.5 GHz spectra from the same sample was an important advantage which we exploit. Standard field modulation techniques were used at 250 and 9.5 GHz, and the power was kept low enough to avoid spectral saturation.

All spectra were taken in the course of cooling the samples from well above $T_m \approx 331$ K to well below $T_g = 243$ K. The temperature control for the 250 GHz spectrometer was provided by flowing water-free nitrogen gas heated or cooled to the appropriate temperature by a home-built unit. In this way, we were able to take spectra at temperatures from about 381 K down to about 123 K. On the 9.5 GHz spectrometer, we took spectra at temperatures from ~ 343 K (well above the melting temperature of OTP) to ~ 213 K, (appreciably below the glass transition temperature). The temperature was controlled by a Varian temperature control unit modified to accommodate the large diameter of our sample. Both temperature control units provided temperature stabilization at the sample to within ± 1 K. Cu-Constantan thermocouples placed near the sample were used to monitor the sample temperature.

The three nitroxide spin probes used in this study vary in size and shape:⁴⁷ 3,3'-dimethylloxazolidinyl-N-oxy-2',3'-5 α -cholestane (CSL) with the nitroxide moiety incorporated into a doxyl ring is a large, cigar-shaped, rigid spin probe with an effective hydrodynamic shape of a prolate spheroid with semiaxes²⁹ $a \approx 12$ Å and $b \approx 3$ Å. Perdeuterated 2,2',6,6'-tetramethyl-4-piperidine-N-oxide (PD-Tempone or PDT) is small and nearly spherical with an effective hydrodynamic radius of 3 Å.⁴⁸ Perdeuterated 2,2',6,6'-tetramethyl-4-methylaminopiperidinyl-N-oxide (MOTA) is approximately spheroidal in shape, consisting of a PDT moiety elongated by a short acetamide chain attached to the piperidinyl ring at the four position.⁴⁷ The nitroxide moiety in these two probes is incorporated into a piperidine ring. We show the geometry and relative sizes of the spin-probes and solvent (OTP) used in this study in Fig. 3.

OTP was purchased from Aldrich and was used without further purification. The perdeuterated spin-probes MOTA and PDT were synthesized locally according to published procedures.⁴⁹ CSL was purchased commercially (Sigma) and used without further purification. The samples were prepared by dissolving a known amount of spin-probe into a known amount of OTP above the melting temperature T_m .

The samples were all at a concentration of approxi-

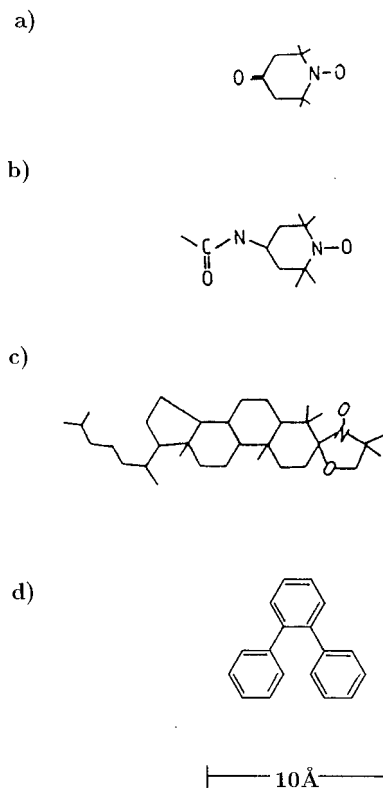


FIG. 3. Geometry and relative sizes of the spin-probes and solvent used in this work: (a) PDT (b) MOTA (c) CSL (d) OTP.

mately 1 mM, which allowed excellent signal to noise at 250 GHz. The samples were sealed in quartz tubes of 6 mm OD and ~ 20 mm in length and degassed by standard, repetitive, freeze-pump-thaw cycles.

Before line shape analysis, the phase of the 250 GHz experimental spectra was adjusted to correct for a slight admixture of dispersion signal. The procedure for correcting the phase is discussed elsewhere.²⁹

III. RESULTS AND GENERAL OBSERVATIONS

Experimental first derivative spectra of PDT, MOTA, and CSL in OTP at 250 GHz are shown in Fig. 1. 9.5 GHz results for PDT and MOTA are shown in Fig. 2. We analyze the 250 GHz spectra quantitatively and use the 9.5 GHz results for general observations.

A. General observations

The following general features can be observed from Figs. 1 and 2. Above T_m , the 250 GHz spectra for PDT have narrow ESR line shapes, characteristic of the fast motional regime, but those of MOTA and CSL show fast motional to incipient slow motional character. As one cools the sample below T_m , there are pronounced differences in the behavior of the line shapes that are correlated with the size of the spin-probe.

At 250 GHz, on cooling, the CSL spectrum changes monotonically into the rigid limit spectrum, i.e., that spectrum which is no longer sensitive to the residual motions of the spin-probes. This rl spectrum is reached well above the glass temperature T_g . The MOTA spectrum also approaches its rl spectrum as the temperature is lowered. There are still small motional contributions present at T_c , however. As the temperature decreases further, a second spectral component appears. The second component is characterized by a much faster dynamical rate than the near rigid limit component. The PDT sample never reaches the rigid limit, even when the sample is cooled to about 123 K, which is well below T_g . The spectra that one observes below T_c are temperature dependent, however. At the lowest temperatures, the line shape is an asymmetric, broad, single line. At higher temperatures, but still well below T_c , the spectra show a poorly resolved two peak structure.

It is difficult to tell from the 250 GHz data alone whether or not the broad PDT line shape is due to the rotational diffusion process or to rapid spin exchange within aggregates of spin-probe. When the sample is heated above T_c , we recover motionally narrowed spectra with no evidence of spin exchange, however. This result suggests that aggregation is not a serious problem at temperatures above T_c .

It is known that the rate of cooling supercooled OTP can influence the formation of polycrystalline domains, particularly in the range⁵⁰ 283–323 K. PDT aggregation in OTP near and above T_c could be related to this phenomenon. Note (i) the background component which is a feature of all of the PDT spectra below 303 K in Fig. 2(a), and that (ii) the spectral extent is considerably less at 303 K than at 323 K. This is due, we believe, to spin-probe aggregation. In one particular PDT experiment that we performed at 250 GHz we were successful in cooling the sample without any sign of spin-probe aggregation in the spectra down to 303 K.⁵¹ For this reason, we limit our present analysis to PDT spectra collected at 303 K and higher, for which we were able to collect spectra with no apparent spin-probe aggregation.

The MOTA and CSL spectra show no evidence of spin-probe aggregation and we were able to analyze data down to T_c without any problems. In fact, we succeeded in obtaining the rigid limit spectra of CSL and MOTA in OTP at 250 GHz that are essential for precise evaluation of \hat{g} and \hat{A} tensors (cf. Fig. 4 and below).

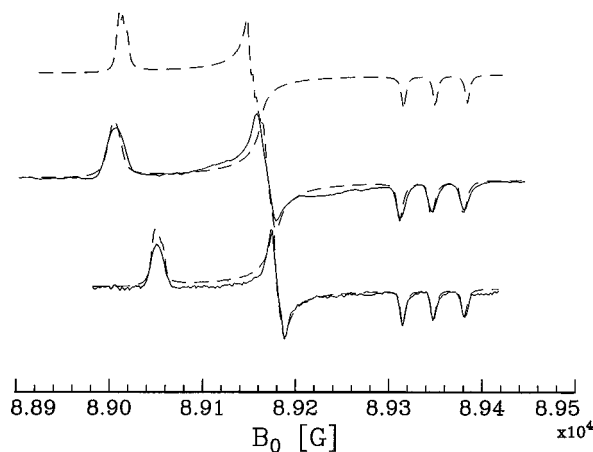


FIG. 4. Fits to rigid limit 250 GHz spectra of (top to bottom) PDT, MOTA, and CSL. The solid lines are the experimental spectra taken at 241 K for MOTA and 228 K for CSL, i.e., sufficiently close to T_g that there are no unresolvable motional features. The dashed lines are best fit simulations.

The 9.5 GHz MOTA spectrum does approach a rigid limit spectrum below T_c . However, careful examination of these spectra also shows a second component that is motionally narrowed below the critical temperature. We believe that the broad feature of the 250 GHz MOTA spectra below T_c can be correlated with the motionally-narrowed component of the 9.5 GHz MOTA spectra. For example, spectral simulations of a typical nitroxide for a rotational diffusion rate of $2 \times 10^9 \text{ s}^{-1}$ yield at 250 GHz a broad spectrum characteristic for smr, while at 9.5 GHz a typical, motionally narrowed three-line spectrum is predicted, (cf. Fig. 5). We will address a possible origin of the second component in the discussion.

B. Spectral simulations

1. Magnetic tensors

Knowledge of \hat{g} and hyperfine (\hat{A}) tensors is essential for successfully extracting the reorientational dynamics of a probe from the ESR spectra. The principal values of \hat{A} and \hat{g} were obtained in the usual way^{29,48} by fitting theoretical simulations to the rl experimental spectrum. The spectra used for this purpose are gathered together in Fig. 4. The values of the magnetic tensors obtained and used in this work are given in Table I. As we have done in previous work,^{29,48,52}

TABLE I. Magnetic tensor parameters.

	g_x	g_y	g_z	A_x^a	A_y^a	A_z^a	β_d
CSL ^b	2.009 010 ^c	0.006 053 ^c	2.002 237 ^c	4.5	4.7	34.2	15
MOTA ^b	2.009 956 ^c	2.006 119 ^c	2.002 239 ^c	4.1	4.9	34.2	0
PDT ^d	2.009 8 ^e	2.006 6 ^e	2.002 2 ^e	4.5	4.9	34.2	0

^aThe estimated error is ± 0.2 G.

^bObtained at 250 GHz from rigid limit spectrum.

^cThe relative error (i.e., the error in g_i relative to a calibration point in the spectrum) is estimated to be 5×10^{-6} for MOTA and 7×10^{-6} for CSL. (The absolute error is dominated by the field calibration error, and it is estimated as 3×10^{-5}).

^dEstimated by scaling results from different solvents, cf. text.

^eThe estimated error is $\sim 1 \times 10^{-4}$.

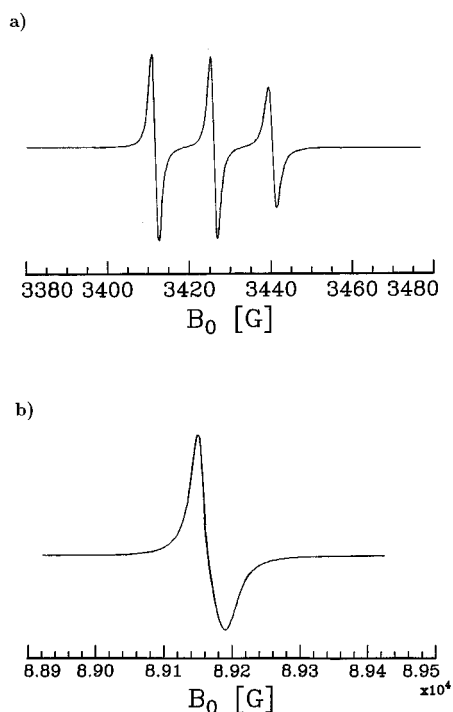


FIG. 5. Simulations appropriate for the fast component ($R^0 = 2 \times 10^9 \text{ s}^{-1}$) of the MOTA spectra below T_g . (a) 9.5 GHz, (b) 250 GHz. Note that the three-line spectrum at 9.5 GHz is a single, broad line at 250 GHz.

we permute the magnetic axes, i.e., the principal axes of the \hat{g} and \hat{A} tensors, of MOTA and PDT so that the magnetic x axis lies along the diffusion z axis, so-called x ordering. CSL spectra, as usual, were fit using a model of y ordering, where the magnetic y axis is permuted to be along the diffusion z axis. In addition, there is a tilt of the magnetic tensors with respect to the diffusion frame, parametrized by the tilt angle, β_d . This tilt is absent in PDT and MOTA and is 15° in CSL. (We use here the nomenclature utilized in the dynamic cage theory³²).

Some comments about these values of magnetic parameters are in order. First, the enhanced sensitivity of 250 GHz EPR to the \hat{g} tensor made it possible to obtain very reliable values for CSL and MOTA from the spectra taken well below the glass transition temperature. Given that we were not able to obtain a rigid limit spectrum for PDT at 9.5 GHz or at 250 GHz, we relied on a scaling procedure for its magnetic parameters. Accurate \hat{g} tensor values for PDT and CSL in toluene are available from previous 250 GHz studies.²⁹ We also have the \hat{g} tensor values for CSL and MOTA derived from rigid limit simulations at 250 GHz from the present study in OTP. To proceed further we make the assumption that the PDT \hat{g} tensor may be scaled from a knowledge of the \hat{g} tensor of PDT in toluene. We used the measured g_x , g_y , and A_z shifts for CSL in OTP compared to toluene to establish a linear extrapolation of the PDT-toluene g and A tensor to values appropriate for PDT in OTP. This is similar to the \hat{A} and \hat{g} scaling used by us in previous work.^{53,54}

For CSL and PDT in OTP it was possible to compare the trace of the hyperfine tensor $3\langle A \rangle$ with the splitting of the

hyperfine lines at 250 GHz in the fmr (i.e., high temperatures). For MOTA, however, the 250 GHz data, even at the highest temperatures, did not extend to fast enough rotational diffusion times to be entirely confident that the splitting of the hyperfine lines accurately represented $\langle A \rangle$, cf. Fig. 1(b).

The 9.5 GHz spectra (uncorrected for dynamic line shifts⁴⁹) have line splittings that are in reasonable agreement with $\langle A \rangle$. If we apply scaling to the \hat{g} tensor, we must also scale the \hat{A} values. A comparison of \hat{g} with \hat{A} shows that whereas g_x and g_y change considerably amongst the three spin-probes, A_z does not. We also note that the scaled PDT magnetic parameters are similar to the MOTA \hat{g} and \hat{A} values. The PDT A_x and A_y values are somewhat arbitrary and are chosen to reflect the measured anisotropy of \hat{A} of PDT in toluene. In any case, $\langle A \rangle$ is chosen to be equal to the measured hyperfine splitting in the motionally narrowed region of PDT at 250 GHz. The small uncertainties in the PDT magnetic tensor parameters are a source of some uncertainty in the determination of the potential well and the rotational diffusion rate for this probe; they have less of an effect on the cage relaxation rate.

The rigid limit tensor parameters for CSL and MOTA were found by using the nonlinear least-squares fitting package described elsewhere⁵⁵ with a very slow tumbling rate.⁵⁶

2. Dynamic parameters

We first compare the spectral fits obtainable with the simple Brownian diffusion model versus the dynamic cage model for 250 GHz spectra over a temperature range where all three spin-probes are sensitive to the details of the model. The dynamic cage model applied to smr ESR by Polimeno and Freed includes the cage-probe interaction potential, $V^{\text{int}}(\Omega)$ generated by the solvent molecules surrounding the probe, where Ω is the solid angle describing the orientation of the probe reference frame with respect to the instantaneous orientation of the cage symmetry axis. For details of the dynamic cage model the reader is referred to.³² The cage potential “seen” by the probe is assumed, for simplicity to be uniaxial and to be approximated by an expansion in the lowest order Wigner rotation matrices, $\mathcal{J}_{mk}^l(\Omega)$ as³²

$$\begin{aligned} -V^{\text{int}}(\Omega)/k_B T &\approx c_0^2 \mathcal{S}_{00}^2(\Omega) + c_2^2 [\mathcal{S}_{02}^2(\Omega) + \mathcal{S}_{0-2}^2(\Omega)] \\ &= \frac{1}{2} c_0^2 (3 \cos^2 \theta - 1) \\ &\quad + \sqrt{\frac{3}{2}} c_2^2 \sin^2 \theta \cos 2\phi, \end{aligned} \quad (1)$$

where θ and ϕ may be taken as the polar and azimuthal angles defining the position of the probe reference frame symmetry or “ z axis” with respect to the cage reference frame. Note that this “lowest order” expansion implies that we can select the principal axes of molecular alignment with respect to the cage.³² To do this we use the known molecular shapes and the results of other studies of these probes in isotropic and oriented fluids,^{29,31–33,47–49,52–54,57} and we discuss them in Sec. IV D.

Comparisons between experimental and best-fit theoretical spectra both for Brownian motion and for the dynamic cage model are given in Fig. 6. In the fits the probe diffusion

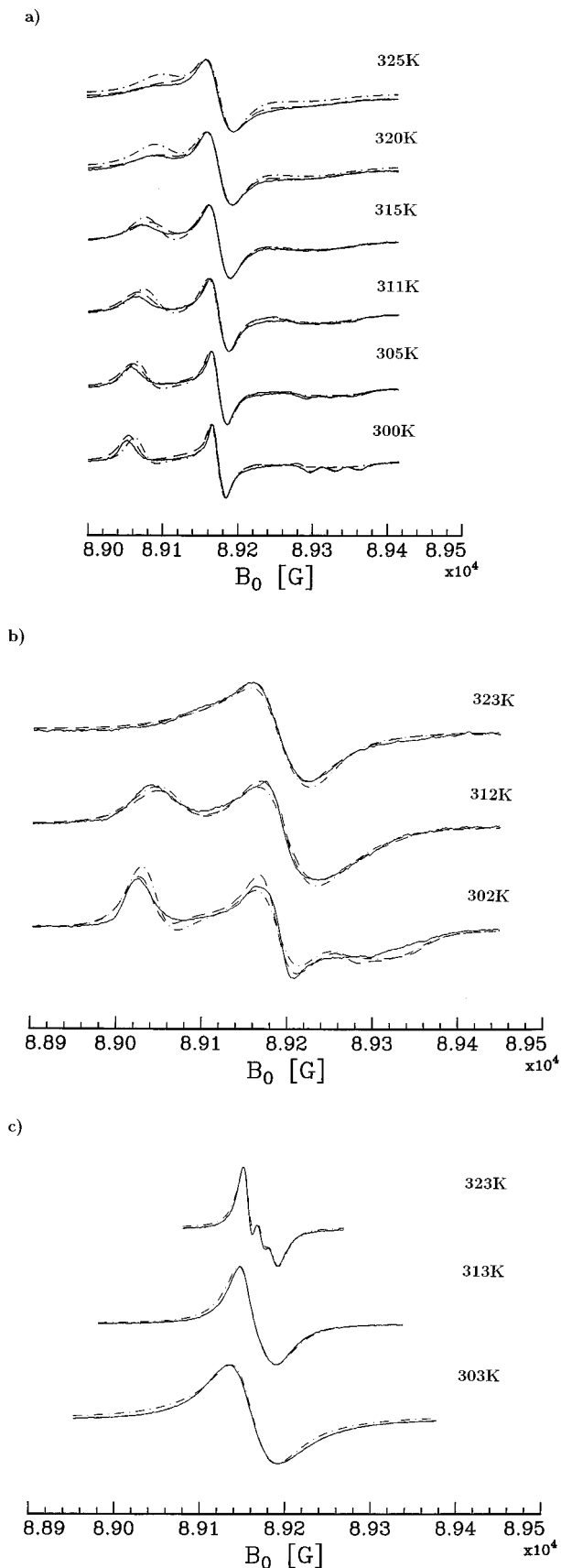


FIG. 6. Comparison of two models for fitting rotational diffusion of spin probes in OTP. (—) experiment, (---) the dynamic cage model, (· · ·) simple Brownian diffusion; (a) CSL; (b) MOTA; and (c) PDT.

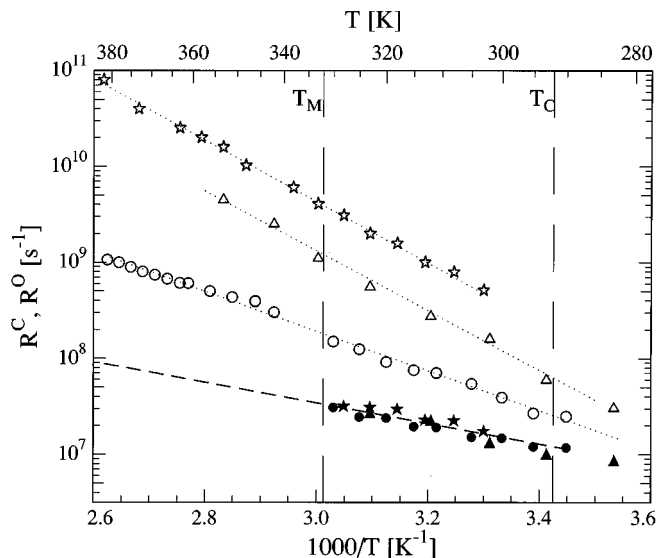


FIG. 7. Dynamic parameters for the cage model: Plot of R^0 (open symbols), the average rotational diffusion rate of the probe and R^c (full symbols), the cage relaxation parameter as a function of inverse temperature for three probes: ☆ PDT, △ MOTA, and ○ CSL. Dotted lines show the Arrhenius fit to the model of simple Brownian reorientation. The dashed line shows an Arrhenius extrapolation for R^c to temperatures above T_m consistent with fits to experiment.

is assumed to be uniaxial and is characterized by the diffusion tensor components R_{\perp} and R_{\parallel} , the former describing the motion of the probe symmetry axis itself (“tumbling”) and the latter related to motion around this axis (“spinning”). For convenience of calculations we introduce the anisotropy ratio, $N = R_{\parallel}/R_{\perp}$ and the mean rotation rate of the probe, $R^0 = \sqrt[3]{R_{\parallel}R_{\perp}^2}$. The cage relaxation rate is given by R^c , and we also have two potential parameters, c_0^2 and c_2^2 , given by Eq. (1). From inspection of Fig. 6, it is clear that the Brownian model is insufficient in fitting key qualitative features of the spectra. The cage model, however, enables good quantitative agreement between experiment and theory. We consider this as solid support for the validity of the dynamic cage model, and in the following analysis we concentrate on the cage model.

The values of R^0 and R^c , and of c_0^2 and c_2^2 that are obtained for each of three spin-probes over the temperature range of this study are shown in Figs. 7 and 8, respectively. All the fit parameters including N for PDT, MOTA, and CSL are collected in Tables II, III, and IV. We found it also instructive to plot the orientational probability function, $P(\theta, \phi) = \exp[-V^{\text{int}}(\theta, \phi)] / \int \sin \theta \exp[-V^{\text{int}}(\theta, \phi)] d\theta d\phi$, with $V^{\text{int}}(\theta, \phi)$ given by Eq. (1) for all three probes, (cf. Sec. IV D).

Some comments about the fitting procedure used in this work are in order. For very efficient nonlinear least-squares analyses of the 250 GHz spectra a modified Levenberg–Marquardt algorithm was applied.⁵⁵ In order to obtain a reliable set of parameters an iterative procedure has been employed. First, we optimized the rotational diffusion parameters: R^0 and N .⁵⁸ The 9.5 GHz spectra were used to check the consistency of the rotational diffusion tensor com-

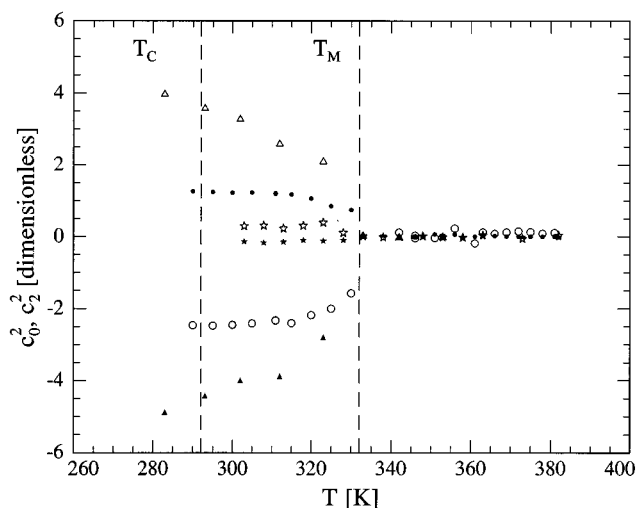


FIG. 8. The Cage potential parameters: Plot of c_0^2 (open symbols) and c_2^2 (full symbols) in units of $k_B T$ vs temperature; \circ CSL, Δ MOTA, and \star PDT. Results above T_m are statistically indistinguishable from zero for MOTA and PDT; for CSL $c_0^2 \approx 0.1$ and is judged barely significant cf. Table IV.

ponents in the fmr.²⁹ Then the cage model parameters were optimized. We found that R^c , c_0^2 , and c_2^2 had the most significant effect on the spectra. Once suitable seed values for all of the relevant dynamic parameters were found in this manner, the constraints were released and we fit all these parameters simultaneously until the optimum set was achieved.⁵⁹ Further details of the fitting procedures are to be found elsewhere.^{32,59}

IV. DISCUSSION

A. Molecular dynamics above T_c

Substantial differences in the mean rotational rates of the probes used in the present study are apparent, cf. Fig. 7. The cigarlike CSL probe rotates nearly two orders of magnitude

TABLE II. PDT. Dynamic cage model parameters.^{a,b}

T (K)	$R^0 \times 10^{-8}$ (s^{-1})	N	$R^c \times 10^{-7}$ (s^{-1})	c_0^2 (kT)	c_2^2 (kT)
303	5.1	1.29	1.7	0.3	-0.15
308	7.9	1.15	2.2	0.3	-0.15
313	10.0	1.10	2.3	0.2	-0.15
318	15.8	1.20	3.0	0.3	-0.10
323	20.0	1.20	3.1	0.4	-0.10
328	30.9	1.20	3.2	0.1	-0.10
333	40.7	1.10
338	60.3	1.15
348	100	1.10
353	160	1.20
358	200	1.15
363	250	1.10
373	400	1.20
382	800	1.15

^aRelative errors in parameters: $R^0 \pm 1.3\%$, $N \pm 5\%$; below T_m : $R^c \pm 2\%$, $c_0^2 \pm 3\%$, $c_2^2 \pm 4\%$.

^bAbove T_m , $|c_0^2| < 0.1$ and statistically indistinguishable from 0; R^c values obtained are thus statistically not meaningful.

TABLE III. MOTA: Dynamic cage model parameters.^{a,b}

T (K)	$R^0 \times 10^{-7}$ (s^{-1})	N	$R^c \times 10^{-7}$ (s^{-1})	c_0^2 (kT)	c_2^2 (kT)
283	3.16	5.62	0.85	4.0	-4.9
293	6.17	5.37	1.01	3.6	-4.4
302	16.6	5.50	1.3	3.3	-4.0
312	28.8	5.88	2.2	2.6	-3.9
323	57.5	6.31	2.7	2.1	-2.8
333	130	6.76
342	265	6.31
353	470	6.46

^aRelative errors: $R^0 \pm 1.2\%$, $N \pm 7\%$; Below T_m , $R^c \pm 3\%$, $c_0^2 \pm 3\%$, $c_2^2 \pm 3\%$.

^bAbove T_m , $|c_0^2| < 0.1$ and statistically indistinguishable from 0; R^c values obtained are thus statistically not meaningful.

more slowly than the small PDT molecule. The MOTA rotational rate is between these two sets of values. On varying the temperature, all probes have dynamics that follow an Arrhenius law from well above T_m down to and just below T_c , with no apparent change at T_m . PDT and MOTA have practically the same “activation energy,” $E_a \approx 14.2 \pm 0.3$ and 13.9 ± 0.3 kcal/mol, respectively which are larger than that for CSL, $E_a \approx 9.0 \pm 0.2$ kcal/mol. The data in Fig. 7 suggest a convergence of the probes’ relaxation rates at lower temperatures, in accord with earlier observations¹⁰ that the mean rotational correlation times of tracer molecules become size independent on approaching T_g (cf. also the references in Fujara, *et al.*¹⁰) indicating an increasing coupling of the probes to their surroundings, which smears out the size difference.

TABLE IV. CSL: Dynamic cage model parameters.^{a,b}

T (K)	$R^0 \times 10^{-7}$ (s^{-1})	N	$R^c \times 10^{-7}$ (s^{-1})	c_0^2 (kT)	c_2^2 (kT)
290	2.45	7.08	1.18	-2.5	1.3
295	2.69	6.17	1.20	-2.5	1.2
300	3.90	6.46	1.48	-2.4	1.2
305	5.50	6.31	1.51	-2.4	1.2
311	7.10	6.76	1.91	-2.3	1.2
315	7.6	6.03	1.95	-2.4	1.2
320	9.3	6.17	2.41	-2.2	1.16
325	12.6	5.89	2.46	-2.0	0.8
330	14.8	5.89	3.09	-1.6	0.7
342	30.2	6.31	3.89	0.1	0.0
346	39.0	6.46	3.98	-0.1	-0.0
351	42.7	5.75	4.07	-0.0	0.1
356	50.1	5.51	4.08	0.2	0.1
361	60.3	5.13	5.01	-0.2	0.0
363	61.7	5.25	5.02	0.1	0.0
366	67.6	4.79	5.13	0.1	0.0
369	74.1	5.13	6.31	0.1	0.0
372	79.4	4.91	6.46	0.2	0.0
375	89	5.01	6.61	0.1	0.0
378	101	4.57	6.61	0.1	0.0
381	107	4.68	8.13	0.1	0.0

^aRelative error: $R^0 \pm 2\%$, $N \pm 7\%$; Below T_m ; $R^c \pm 2\%$, $c_0^2 \pm 3\%$, $c_2^2 \pm 3\%$.

^bAbove T_m , where $|c_0^2| \approx 0.1$, these values are barely statistically significant; R^c values obtained are statistically consistent with the Arrhenius fit shown in Fig. 7 for the results below T_m .

Above T_m the rotational motion of all these probes is adequately fit by a simple Brownian model, and when the dynamic cage model is used, the cage potential parameters are zero to within experimental error, cf. Tables II, III, and IV. It is apparent from Fig. 6 that 250 GHz ESR spectra clearly begin to discriminate between simple Brownian and non-Brownian dynamics of probes upon crossing T_m . Furthermore, PDT, MOTA, and CSL probes are seen from Fig. 14 to experience distinctly different types of cage potential. Nevertheless the slope of R^0 vs T for each probe does not change on crossing T_m , cf. Fig. 7. As the temperature decreases, R^0 of CSL becomes more nearly comparable to the cage relaxation rate, R^c . This is in contrast to the rotational dynamics of PDT and MOTA which are still 1–1.5 orders of magnitude faster at T_c . The faster dynamics and the same activation energies clearly distinguishes the behavior of these two probes from CSL.

Below T_m each of the probes exhibits a substantially different cage potential. Our results indicate that there is some critical probe size that is required for its rotational motion to be significantly influenced by its surroundings. That is, the larger MOTA and CSL spin-probes have cage parameters that sense dynamic or structural changes in the OTP solvent below T_m , whereas the dynamic cage of PDT is very weak, and its rotational motion remains virtually unchanged by the solvent cage below T_m , cf. Fig. 8. Despite these differences, the cage dynamics that emerges from our model fitting is consistent for all the probes. The cage relaxation rate R^c is found, within experimental error, to be the same for PDT, MOTA, and CSL; it is also slower than the spin-probe R^0 and is weakly temperature dependent, with an $E_a \approx 5.0 \pm 0.2$ kcal/mol, see Fig. 7.

B. Correlation functions for the dynamic cage model and stretched exponential fits

Most workers^{10,34,35,60–67} do not report basic relaxation rates as we have done. Rather, they report an “average” correlation time $\langle \tau \rangle$, that results from fitting their motional correlation times to a stretched exponential^{35,68} $G(t) = \exp[-(t/\tau_0)^\beta]$, where τ_0 sets the time scale of the relaxation and $0 < \beta < 1$ is an exponent that characterizes the departure of the relaxation from simple exponential. The average correlation time $\langle \tau \rangle$ is defined as follows for a stretched exponential:

$$\langle \tau \rangle = \int_0^\infty G(t) dt \quad (2)$$

$$= \int_0^\infty \exp(-(t/\tau_0)^\beta) dt \quad (3)$$

$$= \frac{\tau_0}{\beta} \Gamma\left(\frac{1}{\beta}\right), \quad (4)$$

where Γ is Euler’s Gamma function.⁶⁹ In order to check whether our results harmonize with the probe and self diffusion data in OTP obtained by other workers above T_c , we used the dynamic cage model fitting parameters that we ob-

TABLE V. Stretched exponential fit parameters: MOTA.^a

T (K)	β	$1/6\tau_0 \times 10^{-7}$ (s ⁻¹)
283	0.57	3.16
293	0.61	6.17
302	0.63	16.6
312	0.68	28.8
323	0.80	57.5
333	1.00	130.
342	0.99	265.
353	1.00	470.

^aRelative error $\beta \pm 1\%$, $1/6\tau_0 \pm 2\%$.

tained from our ESR spectral fits to generate the correlation function for the probe reorientation in the dynamic cage in the absence of the spin degrees of freedom. These correlation functions were subsequently fit to a stretched exponential. One may then define an average rotational relaxation rate by using the relation $\langle R^0 \rangle = 1/6\langle \tau \rangle$.

The correlation functions corresponding to the particular sets of dynamic cage model parameters were conveniently calculated by modifying our standard programs so that only the probe and cage diffusive part of the stochastic Liouville equation (SLE) was included. This class of correlation functions had previously been calculated by us by a related procedure.^{70,71} Operationally, we set the contributions to the SLE from the magnetic tensors to zero. In addition, we modified the starting vector calculation^{30,71} so that the correlation function of $\mathcal{S}_{00}(\Omega)$ was calculated. Our standard suite of programs⁷² was then used to generate the relevant eigenvalues projected from the modified SLE and starting vector by the Lanczos algorithm. The resulting eigenvalues and weights were then used to generate the correlation function of $\mathcal{S}_{00}(\Omega)$. The resulting function was then fit to a stretched exponential in order to determine the effective τ_0 and β . We give the best fit parameters $1/6\tau_0$ and β in Table V for MOTA and Table VI for CSL.

We show examples of the correlation functions and the stretched exponential fits to them in Fig. 9. A set of curves for three temperatures is shown in which β decreases from unity to less than 0.6 as T is reduced from above the melting temperature to values approaching T_c . Plots are shown for MOTA and CSL. Since PDT relaxes essentially exponentially over the entire data range we analyzed (corresponding to $\beta=1$), it was unnecessary to perform a stretched exponential analysis for this spin-probe. The stretched exponential model fits the MOTA correlation functions rather well. The agreement is reasonable but not quite as good for the CSL correlation functions, and this may be due in part to its ESR spectrum being affected by substantial unresolved hyperfine (shf) interactions with neighboring protons in the molecule. We note that shf interactions are an additional source of inhomogeneous broadening, which reduces the accuracy with which the magnetic tensor parameters may be determined from the rigid limit line shape, and it can reduce the sensitivity to motion in the near rigid limit. These inaccuracies for CSL could contribute to the small differences between the fitting function and the calculated correlation function. On the other hand, there is no fundamental reason

TABLE VI. Stretched exponential fit parameters: CSL.^a

T (K)	β	$1/6\tau_0 \times 10^{-7}$ (s ⁻¹)
290	0.55	2.45
295	0.57	2.69
300	0.60	3.90
305	0.61	5.50
311	0.63	7.10
315	0.70	7.60
320	0.71	9.30
325	0.79	12.6
330	0.90	14.8
342	0.99	30.2
346	0.99	39.0
351	1.00	42.7
356	1.00	50.1
361	1.00	60.3
363	0.99	61.7
366	0.99	67.6
369	1.00	74.1
372	1.01	79.4
375	1.00	89.0
378	1.00	101.
381	1.01	107.

^aRelative error $\beta \pm 2\%$, $1/6\tau_0 \pm 3\%$.

why molecular correlation functions must precisely fit the stretched exponential function.

Finally, Eq. (4) was used to determine the $\langle \tau \rangle$ and hence $\langle R^0 \rangle \equiv 1/6\langle \tau \rangle$, the average relaxation rate for stretched exponential fits. The $1/6\tau_0$ values derived from the stretched exponential fitting function closely follow the probe R^0 values. The increase of the cage potential parameters below T_m as the temperature is lowered leads to a significant decrease in β from 1 to less than 0.6. The temperature dependence of β causes $\langle \tau \rangle$ and $\langle R^0 \rangle$ to deviate significantly from Arrhenius-like behavior as shown in Fig. 10. In fact, $\langle R^0 \rangle$ is much more closely proportional to $1/\eta$ than R^0 , where η is the shear viscosity, consistent with the Stokes–Einstein–Debye (SED) relation, as we discuss in more detail below, (cf. also the $1/\eta$ dependence shown by the dashed and dotted lines in Fig. 10).

The agreement with the SED is best for the MOTA $\langle R^0 \rangle$ values except for the lowest temperatures analyzed. The trend for the CSL $\langle R^0 \rangle$ values is consistent, but there is some departure from the SED prediction as T_c is approached. In our view this could well be caused by the reduced sensitivity of the CSL spectra to the molecular dynamics as the rl is approached.

In order to ensure that our results are not an artifact of the fitting model, we also fit all of our spectra with a simple Brownian model of diffusion, as discussed in Sec. III. We found that the Brownian R^0 values followed a simple Arrhenius law similar to our results using the dynamic cage model as shown in Fig. 7.

Thus, in our view, the average correlation time $\langle \tau \rangle$ should really be regarded as the time integral [cf. Eq. (2)] of a more sophisticated, but homogeneous correlation function for the motion. For our dynamic cage model fit to a stretched

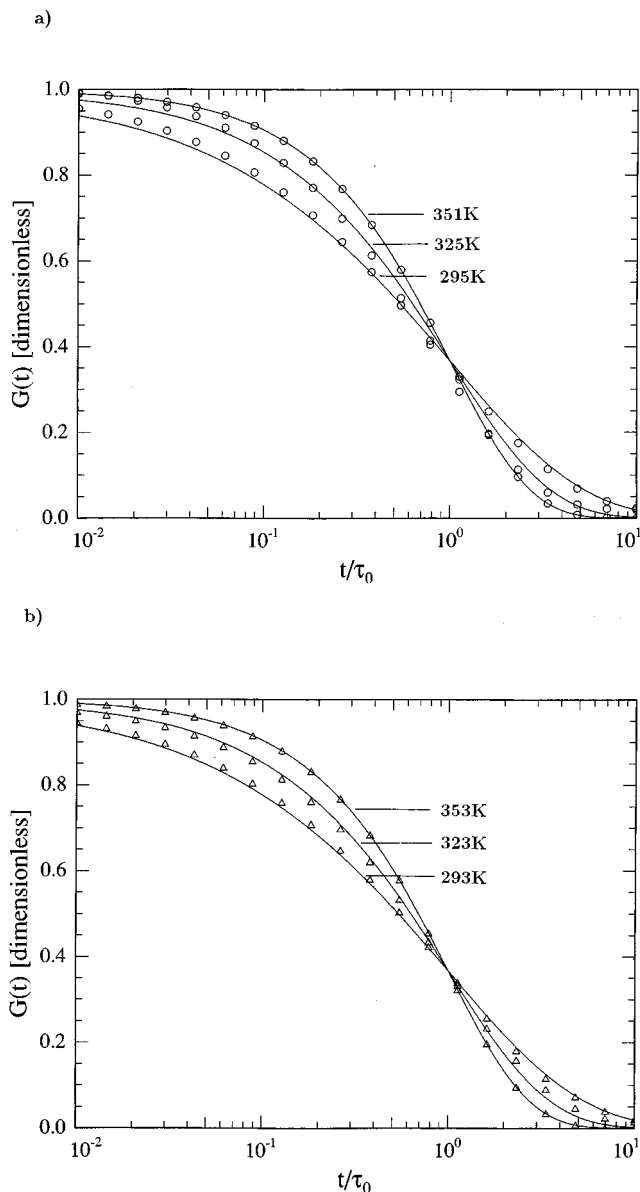


FIG. 9. Calculated correlation functions from dynamic cage model parameters (CSL: \circ ; MOTA: \triangle), and stretched exponential fits (—). (a) CSL. The fit parameters β and τ_0 appropriate to each temperature may be found in Table VI. (b) MOTA. The fit parameters β and τ_0 may be found in Table V.

exponential, β is a measure of the extent of the coupling of the probe dynamics to that of the cage.

A stretched exponential with $\beta \neq 1$ has typically been taken in the past to imply a distribution of correlation times leading to nonexponential relaxation,^{35,68} i.e.,

$$\exp\left(-\left(\frac{t}{\tau_0}\right)^\beta\right) = \int_0^\infty \exp(-t/\tau) \rho(\tau, \tau_0; \beta) d\tau, \quad (5)$$

where $\rho(\tau, \tau_0; \beta)$ is the probability distribution in relaxation times τ . In Fig. 11 we show distributions of correlation times in $1/\sigma \equiv \tau/\tau_0$ corresponding to various values of $0 < \beta < 1$. More generally, there has been a long-standing question^{10,73,74} whether the nonexponential relaxation is homogeneous (consistent with our above analysis), in which

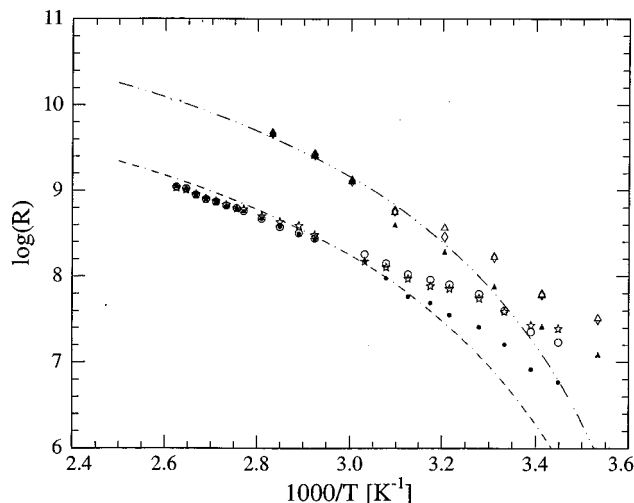


FIG. 10. Parameters from fits of motional correlation functions to a stretched exponential. We plot the average rotational diffusion rate ($R^0 \equiv 1/6\langle\tau\rangle$) (with $\langle\tau\rangle$ defined by Eq. (4) and $1/6\tau_0$ (cf. Tables V and VI), for CSL and MOTA. The values of R^0 from Tables III and IV are shown for comparison. \triangle MOTA $1/6\tau_0$; \blacktriangle MOTA $1/6\langle\tau\rangle$; \diamond MOTA R^0 ; \circ CSL $1/6\tau_0$; \bullet CSL $1/6\langle\tau\rangle$; \star CSL R^0 ; (---) is the SED prediction for the rotational tumbling rate of CSL; (- - -) is the SED prediction for MOTA; both SED predictions are proportional to $1/\eta$.

case all regions of the sample would show the same nonexponential relaxation, or whether the relaxation is inhomogeneous with a distribution of sites relaxing exponentially, yielding an overall nonexponential behavior.

We determined the distribution of relaxation times $\rho(\tau, \tau_0; \beta)$ that would reproduce the stretched exponential fits.⁷⁵ If we follow the often invoked Ansatz^{10,35,37} that the stretched exponential implies that the relaxation is heterogeneous, and we write the relaxation function in the form of Eq. (5), then we may calculate the ESR spectrum associated with a particular distribution of relaxation times as follows

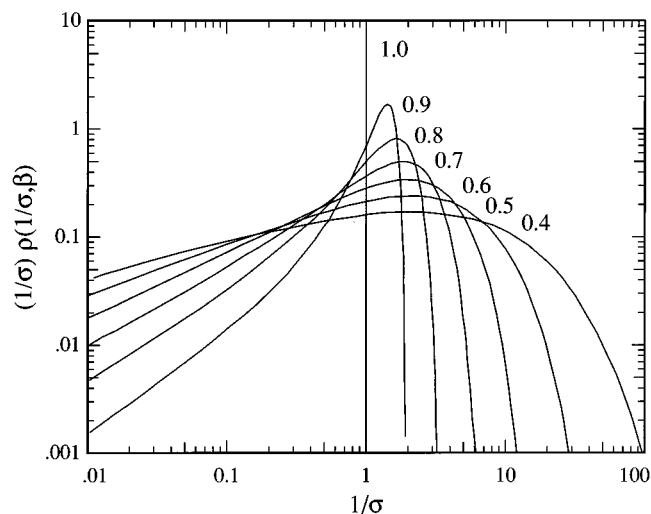


FIG. 11. Plot of weighted distributions in $1/\sigma \equiv \tau/\tau_0$ (cf. text) for various values of the parameter $0.4 \leq \beta \leq 1$. As β approaches one, the distribution of relaxation times becomes narrower.

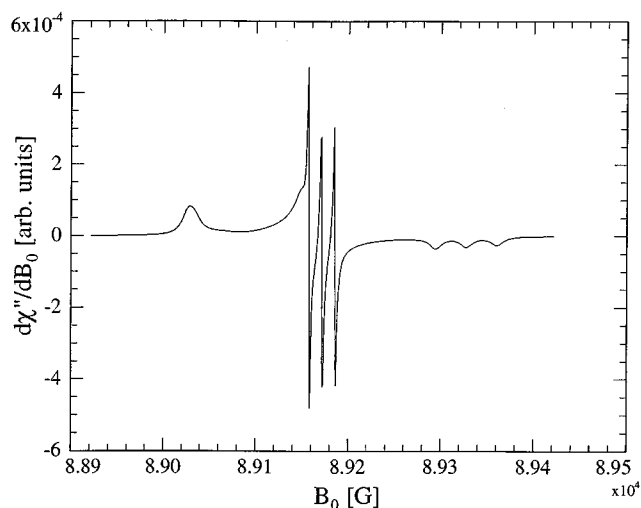


FIG. 12. 250 GHz spectral simulation based on an inhomogeneous distribution of correlation times according to Eq. (5), and parametrized by the exponent $\beta=0.6$. (The stretched exponential function fit was to the correlation function corresponding to CSL at 27 C, cf. text.)

$$I(\omega; \tau_0, \beta) = \int_0^\infty I(\omega; \tau) \rho(\tau, \tau_0; \beta) d\tau, \quad (6)$$

where $I(\omega; \tau_0, \beta)$ is the predicted ESR spectrum corresponding to the stretched exponential parameterized by τ_0 and β , and $I(\omega; \tau)$ is a spectral component relaxing by simple reorientational diffusion, characterized by a Debye relaxation function i.e., $\beta=1$. To accomplish this, a series of model slow-motional ESR spectra were calculated assuming simple diffusion. The weighted sum of the model spectra that were approximately equally spaced in the variable $\log(\tau/\tau_0)$, was then computed to generate $I(\omega; \tau_0, \beta)$.

This is consistent with an inhomogeneous distribution of domains relaxing exponentially, but yielding a ‘‘composite’’ spectrum described by a nonexponential decay. Figure 12 shows the result of such a calculation at 250 GHz. The parameters used in the calculation were appropriate for CSL at 27 C. A comparison of the model spectrum shown in Fig. 12 and the experimental spectrum in Fig. 1 at 27 C shows that the contribution from rapidly tumbling components produces sharp features in the stretched exponential model spectrum that are simply not present in the experimental spectrum. We have performed this same exercise for a variety of cases corresponding to the different spectra in Figs. 1(b) and 1(c), and we always obtain spectra with the characteristics of Fig. 12, that are inconsistent with experiment. (We do find that summation spectra taken on a denser grid over values of τ/τ_0 in the motional narrowing regime, do broaden somewhat the contribution from the rapidly tumbling regime, but the key spectral characteristics do remain independent of grid size. It is the assumption of a spread of correlation times that is the most important feature of the analysis.) We take this as strong evidence that the relaxation in the supercooled state is homogeneous above T_c . This conclusion also appears to us to be the most reasonable. After all, this is the region of a

supercooled liquid where MOTA and CSL reorientation rates are, $6R^0 \approx 10^{10} - 10^8 \text{ s}^{-1}$ consistent with quite rapid molecular relaxation.⁷⁶

C. Comparison with the results from other techniques

We are now in a position to compare our molecular dynamics results with the results obtained from other spectroscopies. In order to do so, we shall convert translational diffusion results of other workers into an equivalent average rotational relaxation rate by a procedure we now describe.¹⁰

It has become commonly accepted to interpret molecular diffusion of individual molecules in a wide range of liquids above the melting point ($T \geq T_m$) and to some extent also in the supercooled state ($T \geq T_c$) in terms of the basic Stokes–Einstein relation for translational diffusion

$$D(T) = \frac{k_B T}{6\pi\eta(T)r_e}, \quad (7)$$

and the Debye equation for rotational diffusion

$$R(T) = \frac{k_B T}{8\pi\eta(T)r_e^3} \quad (8)$$

(SED),^{77–80} where D and R are the translational and rotational diffusion constants, respectively, k_B is the Boltzmann constant, $\eta(T)$ is the shear viscosity of the substance of interest, and r_e is the mean hydrodynamic radius of the moving molecule. In light of the success of the SED in rationalizing self and tracer dynamics in simple liquids, Eqs. (7) and (8) have frequently been employed in studying deviations of molecular dynamics from SED on lowering the temperature and/or raising the pressure.^{10,14,23,35,43,53,54,63,65,81} In order to convert D^{OTP} to an “equivalent rotational rate”, we make use of SED and multiply D^{OTP} by a conversion factor, $3r_e^{-2}/4$, cf. Eqs. (7) and (8), with $r_e \approx 4.13 \text{ \AA}$.⁶⁵ Such a scaling is justified in the temperature range of present interest since a decoupling of translational and rotational dynamics reported in the literature takes place at appreciably lower temperatures.^{10,14–16} The self-diffusion translational coefficients, D^{OTP} are taken from Hahn echo NMR data,⁸² since they are tabulated and they are in excellent quantitative agreement with recent static gradient and pulsed gradient stimulated echo ^1H –NMR and (via SED) with ^2H –NMR molecular reorientation studies.^{10,62,63} Also the temperature dependence of the OTP viscosity used for comparison is conveniently given by a phenomenological equation of Cicerone and Ediger.⁴²

Coherent neutron scattering^{26,83} and depolarized light scattering^{27,65} studies reported the existence of two relaxation processes above T_c , the slow α -process consistent with the results of other methods,^{10,27,43,64–66,82} and a fast, less well-defined process on the ps time scale.^{26,27,65} Depending on how the data are analyzed, the fast process is found to be either temperature independent,⁶⁵ or to some extent to follow the predictions of MCT.⁶⁶ As an example, results from light scattering studies⁶⁵ are included in Fig. 13. The relaxation times of both processes, τ_α and τ_β are converted to the ro-

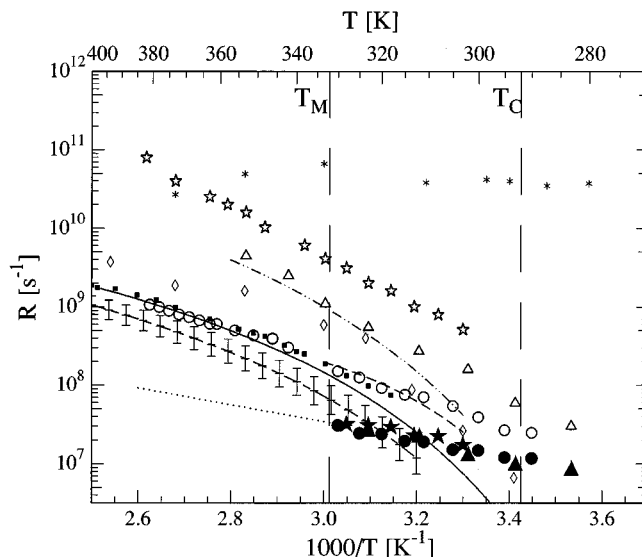


FIG. 13. Comparison of the temperature dependence of different relaxation rates obtained by various experimental techniques scaled to an equivalent rotational tumbling rate as discussed in the text. Time correlated single photon counting data of Cicerone *et al.* (Ref. 35) (---) anthracene; (---) anthanthrene; (---) mean behavior of rubrene, DPA, DANS, and BPEA (vertical bars indicate range of values characteristic for these optical probes). ■: rotational rates calculated from translational self diffusion NMR data of McCall *et al.* (Ref. 82) (cf. text); (—): mean viscosity behavior from (Ref. 35) (vertically shifted to coincide with $\log R^0$ of the CSL data). Light scattering data of Steffen *et al.* (Refs. 27 and 65) \diamond slow process, and * fast process. Other symbol codes as in Fig. 7 for ESR results from this work.

tational rates assuming $R = (6\tau)^{-1}$. Whatever the origin of τ_β , it is the fastest of all processes shown in Fig. 13, and it does not visibly correlate with the rotational rate of any probe.

At temperatures above T_m , the diffusion rates of our probes are consistent with results for OTP self diffusion⁸² and other tracers used in time resolved optical spectroscopy.³⁵ Notably, the rotational rate of CSL coincides with the self diffusion constant of OTP. Probes used as optical tracers are generally larger, multiring molecules, and they can be divided into two categories: Those which are extended in space, ramified and, thus, partially flexible, e.g., rubrene, and those which are flat orthorhombhedron- or disklike such as anthracene or anthanthrene, cf. Fig. 1 of Cicerone, *et al.*³⁵ Not surprisingly the rotational rates of tracers belonging to the former category are smaller than that of CSL. The flat probes reorient at faster rates, with the disklike anthanthrene reorienting at similar rates as CSL, while the flat orthorhombhedronlike anthracene is closer in diffusional behavior to MOTA.

Note that by plotting the “average probe rotational tumbling rates” $\langle R^0 \rangle$ we improve the agreement considerably between our results and those of other workers^{10,34,35,60–67} versus the actual measured rotational tumbling rates, R^0 , (cf. Fig. 10). An advantage of our study is that the experimental ESR spectra, and the model used to fit them, allow us to make a detailed study of the local molecular dynamics in ways that are inaccessible to spectroscopies that take a stretched exponential correlation function as a given and do

not enable one to explore the mechanism of the nonexponential decay. To address this point we now discuss our dynamic cage parameters in more detail.

D. Description of the dynamic cage

Our results have shown that PDT reorients rapidly and only experiences a weak dynamic cage. The larger spin-probes MOTA and CSL experience a significant dynamic cage below T_m . We also have observed that MOTA not only reorients much faster than CSL but it also features a substantially different cage potential. The results given in Tables III and IV, and shown in Fig. 8, reveal the initially surprising fact that while the ordering of the MOTA long axis with respect to the cage symmetry axis is positive (i.e., $c_0^2 > 0$), the CSL long axis ordering is negative ($c_0^2 < 0$), the latter result being in contrast to the positive macroscopic ordering it exhibits in liquid crystalline media^{31,33,47,52} and the positive ordering it exhibits in the dynamic cage of a liquid-crystal solvent.³³ To study the meaning and significance of these findings we first plotted the orientational probability function for the molecule with respect to the cage, i.e., $P(\theta, \phi)$ in polar coordinate form, $[P(\theta, \phi), \theta, \phi]$. The resultant probability surface together with the Cartesian reference frames $[x', y', z']$ for CSL, MOTA, and PDT are shown in Fig. 14.

Note that above T_m there is no significant dynamic cage as reported by the potential parameters. As we argue below, this is due to the absence of local structure (in the sense of Kivelson and co-workers^{17,18}) and we assume that the spin-probes are reorienting in an isotropic medium. Below T_m , we assume that a local structure grows in as the temperature is lowered, and we identify the local structure with the dynamic cage. In order to rationalize our data, the local structure must have the following properties:

- 1) There are voids in the local structure sufficiently large for the PDT spin-probe to tumble freely. We offer a possible interpretation of these voids in terms of defect propagation in Sec. IV F.

- 2) The voids are not so large that the MOTA spin-probe may tumble freely. Although the activation energy is similar for PDT and MOTA, we postulate that it is the acetamide tail of the MOTA spin-probe that prevents MOTA from tumbling freely. This is consistent with MOTA having a hydrodynamic radius between that of PDT and CSL, which is plausible on steric grounds, and is roughly equal to that of OTP (hydrodynamic radius⁶⁵ 4.13 Å).

- 3) The oblong CSL spin-probe prefers to lie along the x axis of the dynamic cage, indicative of a “discoticlike” ordering.³²

OTP is a nonplanar molecule, however, and is incapable of sustaining long-range discotic order. Nevertheless, a consistent model may be put forth by assuming that OTP packs locally like a discotic, where the “mesogen” units may be thought of as having the shape of a nautilus shell.³⁷ This simple picture accounts for the nonplanar character of OTP. If we were to put such units on a bcc lattice with a lattice constant approximately equal to two OTP hydrodynamic radii,⁶⁵ i.e., 2×4.13 Å, and the “origin” of the nautilus

shells on the lattice points, then we can account for the PDT and MOTA results by removing an OTP molecule from the center of the bcc lattice and replacing it with a PDT or MOTA spin-probe. PDT will diffuse freely in the large void. The MOTA results indicate that the bcc lattice departs somewhat from cubic symmetry. If the central molecule of the bcc lattice is removed, it is possible that, locally at least, the two planes of nearest neighbors to the void move toward one another along the “discotic director” orientation. In this picture, MOTA can rotate freely in a plane parallel to the discotic director and containing the lattice point of the removed “mesogen unit”.

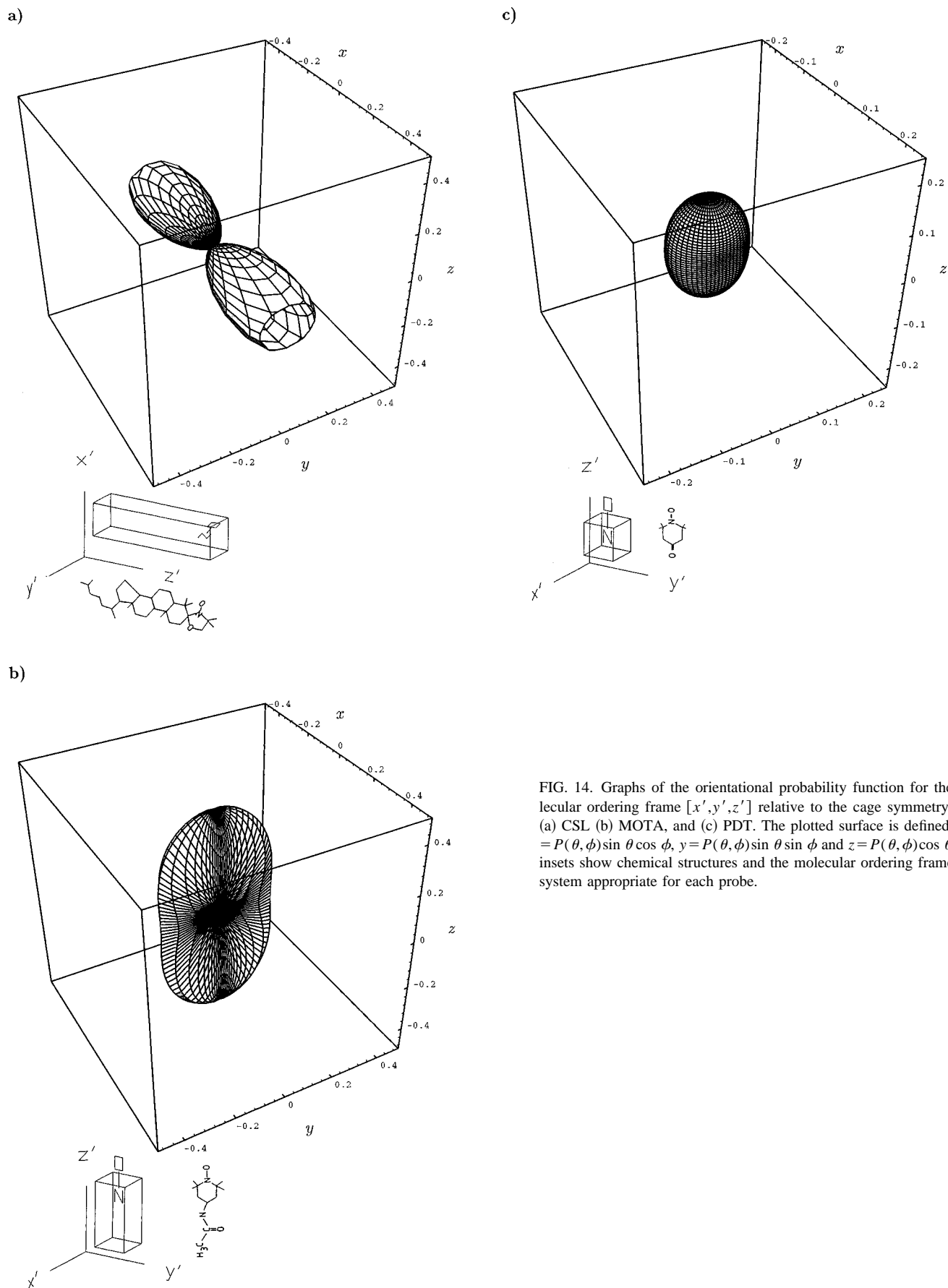
We estimate below that the dynamic cage experienced by our spin probes consists of approximately ten nearest neighbors, which is consistent with our simple postulate of a bcc lattice. Our model for CSL is only slightly more complicated. Here we assume that two adjacent bcc ‘unit cells’ are involved. In this case, we remove both central lattice mesogens and insert a CSL molecule in the void. This simple picture has the correct symmetry to accommodate our CSL data.

Although this picture is necessarily qualitative, it does rationalize our data. Moreover, it is consistent, as we show below, with estimates of the number of participating neighbors in the dynamic cage. The model can also rationalize why the cage diffusion rate is the same for all spin-probes. We view the dynamic cage as a sort of matrix “condensation” around the guest molecule, and this condensation very likely involves only the nearest neighbors of the probe, as we argue based on the model of Kivelson and co-workers.^{17,18,84}

We also wish to emphasize that experiments^{50,85} and molecular dynamics studies^{34,86} do not indicate any differences in OTP behavior from that of a normal liquid on crossing T_m . In particular, no change in the specific volume,^{34,50,86} the specific heat,⁸⁵ or the excess configurational entropy⁸⁵ on crossing T_m have been observed. The Kivelson model and our results are consistent with this behavior.

Since PDT, MOTA, and CSL have distinctively different sizes and shapes, some comments as to why the cage relaxation rate is the same for all probes are in order. First, we note that if the probe is of the size of a matrix molecule, then the cage should relax on the time scale characteristic of, e.g., dielectric or viscoelastic relaxation referred to the cooperative motion of a limited number of nearest neighbors,⁸⁷ within some rough distance from the domain center (or the probe). In this picture, we interpret R^c as the rate at which diffusional events within the solvent cause the dynamic cage to change its orientation.⁸⁸ Our results suggest that the sizes and shapes of MOTA and CSL are in this regime, and a comparable number of the neighboring OTP molecules should be involved in relaxing their cages.

It is, therefore, tempting to make an approximate estimate of the number of molecular events taking part in the dynamic cage relaxation. If we assume that the dynamic cage maintains its orientation on a time scale set by diffusional events of the solvent in the probe neighborhood, we may relate R^c to the translational diffusion constant of OTP by a relation of the form $R^c \approx D^{\text{OTP}} d^{-2} n^{-1}$ where $D^{\text{OTP}} d^{-2}$ is the



displacement frequency, d is the minimum significant translational displacement length and is of the order of the r_e of OTP. Also, n is an estimate of the number of translational diffusion steps of the solvent that are required. D^{OTP} used in the above relation should be a microscopic diffusion constant rather than the macroscopic one. For such an estimate the self-diffusion data of McCall *et al.* can be used.⁸² Recent molecular dynamics simulations³⁴ have shown that mean molecular displacements of the order of r_e are accomplished in OTP on a time scale of a few ps (at high temperatures) to a few tens of ps (at lower temperatures), and on those time scales the diffusion constant has already reached its long-time asymptotic value. The very good agreement between the temperature dependence of the simulations and the self-diffusion coefficients (cf. Table II and Fig. 4 of McCall *et al.*⁸²), at high temperatures suggests that D^{OTP} values⁸² can be used in the estimate of n over the temperature range of interest. With R^c from our results and $d \approx 4.13 \text{ \AA}$,⁶⁵ one finds n of the order of 10 and weakly decreasing on cooling from 390 to 330 K.

E. The frustration-limited cluster size model

Our estimate of the solvent cage size is consistent with the growth of a frustration-limited cluster size proposed by Kivelson and co-workers,^{17,18,84} (cf. Sec. I). That model uses a dynamic scaling argument to write such properties as the shear viscosity, η or the average relaxation time, $\langle \tau \rangle$ as follows

$$T \log[\langle \tau \rangle / \tau_0] \approx T \log[\eta / \eta_0] \approx BT^* \epsilon^{4\nu}, \quad (9)$$

where $\nu = 2/3$ for ordinary three-dimensional critical phenomena, τ_0 and η_0 are molecular quantities described by an activation energy

$$\eta_0 \approx \eta_\infty \exp[E_\infty / k_B T], \quad (10)$$

$$\tau_0 \approx \tau_\infty \exp[E_\infty / k_B T], \quad (11)$$

where η_∞ , τ_∞ , and E_∞ , are all species dependent quantities characteristic of the fluid state above T^* , B is a measure of the degree of frustration in the system, and ϵ is the reduced temperature

$$\epsilon = \frac{T^* - T}{T^*} \quad (12)$$

For OTP, the parameters are¹⁸ $T^* = 350 \text{ K}$, $B = 412$, and $E_\infty = 6.25 \text{ kcal/mol}$. This activation energy is consistent with but slightly larger than the dynamic cage activation energy $E_a = 5.0 \pm 0.2 \text{ kcal/mol}$ we infer from our nonlinear least-square fits.

Note that the molecular time scale τ_0 and the molecular quantity η_0 are both described by an activated process. From our dynamic cage model analysis, we note that the probe and cage diffusion rates are also described by activated processes. It is the average quantity $\langle \tau \rangle$ and the macroscopic shear viscosity η that show departures from simple activated behavior. Furthermore, above T^* , the right hand side of Eq. (9) vanishes, which forces $\langle \tau \rangle$ and τ_0 to have the same temperature dependence via the logarithm on the left hand side

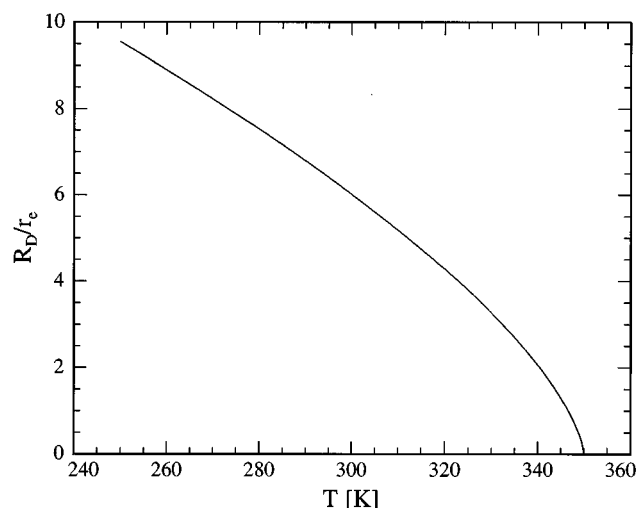


FIG. 15. Plot of the temperature dependence of the frustration-limited domain size R_D using parameters appropriate for OTP [cf. Eq. (14)].

of Eq. (9), in agreement with our rotational tumbling results, where we find that our high temperature spectra are well described by a correlation time with an Arrhenius temperature dependence.

The concept of a domain size is also useful for explaining the ‘‘turn on’’ of the cage potential as reported by the nonlinear least-squares analysis as the temperature is lowered. In the frustration model, the frustration-limited domain size $R_D \propto \epsilon^\nu$. Kivelson and co-workers¹⁷ estimate that $R_D \approx 10r_e$ at the glass transition temperature, where r_e is the size of an OTP molecule. Thus, at the glass transition temperature roughly $(R_D/r_e)^3 \approx 1000$ OTP molecules are in a frustration limited domain size. Assuming that R_D may be written as follows:

$$R_D(T) = R_g \left(\frac{T^* - T}{T^*} \right)^\nu, \quad (13)$$

$$R_D(T_G) = 10r_e,$$

we may solve for R_g to find the temperature dependence of R_D . We find

$$R_D(T) = 22r_e \left(\frac{350 - T}{350} \right)^{2/3}. \quad (14)$$

Figure 15 shows the predicted temperature dependence of R_D . At T^* , R_D vanishes. From the estimate computed above, where we found $n \approx 10$, we may infer that ~ 10 diffusion steps are required to relax the cage below T_m . At 330 K, where the cage potential begins to become significant, we estimate that $R_D \approx 2.5r_e$ or that there are $(R_D/r_e)^3 \approx 16$ molecules in a frustration limited domain. This is in qualitative agreement with our estimate for n .

We suggest that below a certain minimum value of R_D the domain size is too small to support a significant dynamic cage. As the temperature is lowered and the number of molecules within R_D increases, it is possible for the probe molecule to experience a significant dynamic cage and the potential parameters describing the depth of the cage ‘‘well’’

increase to reflect this correlated behavior. As R_D continues to increase, the probe molecule, which is coupled most tightly to its nearest neighbors, experiences a potential which “saturates” as the probe loses dynamic contact with the frustration limited domain boundary. Within the domain, fluctuations described by the coherence length $\xi_0 \propto \epsilon^{-\nu}$ become shorter and shorter as the temperature is lowered and may be responsible for the slight temperature dependence of the number n of diffusion steps required to relax the cage as T_c is approached.

F. Two-component features in the PDT and MOTA ESR spectra

We would now like to discuss features of our experimental spectra below T_c which provide evidence for a discrete type of heterogeneous relaxation. That is, this heterogeneity reflects discrete types of spin–probe interaction with the solvent cage, rather than, e.g., a distribution of independently relaxing domains in the solvent.⁸⁹ The temperature variation of the 250 and 9.5 GHz ESR spectra below T_c provide us with qualitative information about the dependence of the solvent cage on probe size. As we have already discussed, the spectra of our smallest probe, PDT are consistent with that of an almost freely diffusing molecule down to the lowest temperatures studied, cf. Figs. 1(a) and 2(a). Additionally, if the OTP sample is not annealed for sufficiently long times at high temperatures, $T \gg T_m$, before cooling down, the spectra show evidence of Heisenberg spin exchange characteristic of PDT spin–probes constrained to be in close proximity, [cf. Fig. 2(a) and the discussion in Sec. III A]. The spectra of MOTA, which is roughly almost twice as large as PDT, are in turn, a superposition of two components originating from two kinds of species each reorienting with a distinctly different rate. On lowering the temperature, the slower component in the MOTA spectra converges to the rigid-limit spectrum, while a contribution from the fast moving species behaves in a similar manner to that of PDT spectra, cf. Figs. 1(b) and 2(b). As we argue below, these observations imply characteristics in the behavior of PDT and MOTA, that originate from the same structural properties of the OTP matrix.

In the absence of any additional experimental or theoretical evidence on the matter, we present schematic, intuitive 2D arguments based on a densely packed OTP matrix (corresponding to a temperature close to T_g), which help to rationalize these findings, without attempting a specific arrangement of the probe molecules in OTP below T_c . We find that it is simplest to interpret our results below T_c in terms of such a model involving dense packing which is in contrast to the relatively open bcc lattice structure that we utilized for the frustration-limited cluster-size model. One could argue that this is consistent with the reduction of the free volume in the supercooled liquid as the temperature is lowered. This might also be consistent with a disruption of the locally ordered structure of a cluster.

Let us consider a simple 2D hexagonal network, with the intersite distance equal to that between phenyl rings of OTP,

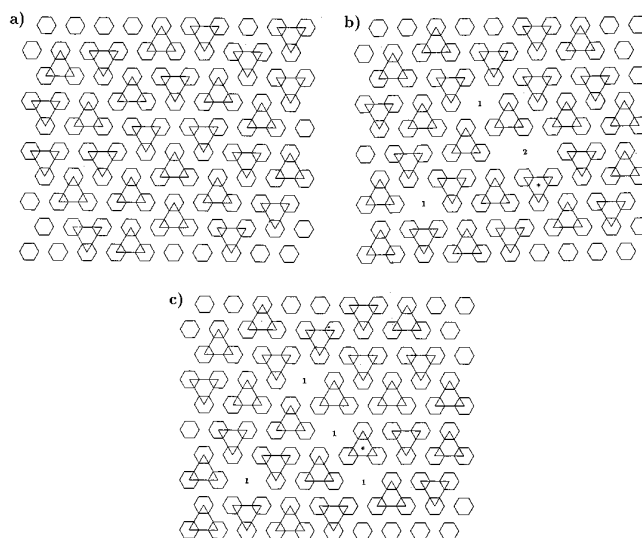


FIG. 16. 2D hexagonal model showing the presence of single site and double site defects. The dense packing indicates (qualitatively) a temperature near T_g . (a) A random distribution of triads of phenyl groups, representing a two-dimensional, densely packed, random tiling of OTP molecules. (b) A system with two single site defects (marked 1) and one double site defect (marked 2). The molecule marked with an asterisk can flip about the edge bordering on the double site defect to convert it into two single site defects. (c) Conversion of a double site defect into two single site defects via a molecular “flip” around the axis defined by the “edge” of the OTP molecule marked with an asterisk [cf. Fig. 16(b)]. Molecular flipping about other molecular edges can cause two single site defects to coalesce into a double site defect.

see Fig. 16. Each OTP molecule occupies three adjacent sites on the network. We assume additionally that OTP phenyl rings are undistinguishable, therefore rotational dynamics about any of the symmetry axes does not change the position of the “particle” on the network. This is visualized by drawing equilateral triangles joining the adjacent sites wherein each of the three sites is one of the phenyl rings. In Fig. 16(a) the close packing limit (cpl) is presented. Note that in the cpl with random orientation of the particles, each “molecule” has 6 ± 1 neighbors, and that the minimum size of a defect on the network will be of the size of a phenyl ring. Let us now create a void in the system by removing one of the triangle particles representing the removal of a single OTP molecule. The neighboring phenyl rings can move into the void space either by (i) translation into the void—and this can only happen to a molecule which is not sterically prevented from doing so by the other molecules—or by (ii) a “flip–flop” about one of the triangle’s edges. Whereas only (i) can yield a new void of three sites, both (i) and (ii) can split the void into two smaller defects: A single and a double site one. Repetition of (ii) can split the double site into two single site defects, as we show in Figure 16(c).

If we put a PDT probe molecule into the proposed system, it will occupy a vacant site, i.e., a single site defect, which will introduce only a limited amount of frustration in the system because of the size compatibility. The PDT probe will be surrounded by either four or five particles in 2D. Rotationally, the probe should remain essentially decoupled

from the matrix, e.g., reside in the form of an isotropic cage formed by the surrounding particles. The translational dynamics will be governed by a highly cooperative process of defect diffusion involving an orchestrated effort of several particles to bring a defect to the probe neighborhood. The larger the number of cooperatively involved particles, the larger the distance the defect has to travel before reaching the probe. Thus, translational diffusion of the single site probe is controlled by defect diffusion and the number of defects in the system.

This brings us to two observations. The first is that two PDT-like probes brought together on our network will have difficulty separating from one another, even if we ignore possible attractive forces between them. If a single site defect encounters the pair, the probes will probably prefer to diffuse inside the enlarged cage rather than separate because of the substantial difference between the inertia of the probe and an OTP molecule. Only an encounter with two or more defects simultaneously can create a sufficiently large void to allow the aggregate to separate. This would help to explain the Heisenberg spin-exchange broadening in low-temperature spectra of PDT.

The second observation is that for a larger, double site probe (e.g., MOTA) not only translational but also rotational dynamics would require a strong cooperative effort with the surroundings to facilitate reorientation of the probe, as argued by, e.g., Matsuoka and Quan.⁸⁷ This probably explains the two-component feature of the MOTA spectra. This probe can fit into either a single or double site vacancy, with 5–7 surrounding particles. The single site occupancy would require, however, some kind of local structural adjustment in the hexagonal network to accommodate the tail chain. Consequently, any reorientation of the probe in this case requires an orchestrated effort of the probe and surrounding particles. It is important to note that the local positional adjustment of OTP molecules and the dynamic cooperativity requires, in our model, the involvement of only a few of the nearest neighbors. The rotational dynamics changes, however, when a defect encounters the probe and the probe has a double site vacancy at its disposal. The probe gains sufficient space to rotate freely in a manner similar to PDT, as long as the local rearrangements do not remove the defect, and this should be difficult as we argued above. These distinctly different surroundings, if present, give rise to two different time scales for the rotational dynamics, a slow, cooperative one and a fast one, characterized by rapid tumbling in a steric cage. The relatively large population of double site and larger size voids seems to persist, probably even to temperatures far below T_c , as manifested in our MOTA spectra, cf. Figs. 1(b) and 2(b) and the discussion in Sec. III A. An estimate of the fraction of probes taking part in each of the processes is beyond the scope of the present paper.

Although the MOTA spectra suggest relatively large, double site and perhaps even larger voids below T_c , there is a limit to the stable void size, as evidenced by the absence of void-driven aggregation of MOTA and CSL in the experimental spectra. We do not discuss the accommodation of the CSL probe on our hexagonal network, but it is clear from the

behavior of the slow cooperative mode in the MOTA spectra, that this should be the prevailing mechanism for the dynamics of CSL. A void of the volume of two adjacent OTP molecules would be sufficient to comfortably accommodate CSL, and we find 7 to 8 OTP molecules surround such a void on the network.

Although the discussion of this subsection emphasized heterogeneity due to the probe in the region $T < T_c$, results from other spectroscopies indicate the importance of solvent heterogeneity below T_c , a matter we wish to address⁹⁰ in the context of a more detailed analysis of our ESR spectra below T_c . However, it is appropriate to note that significantly below T_c , the spectra lose their sensitivity to R^c , because it becomes too slow. This is equivalent to saying that, in the time scale of the 250 GHz ESR experiment, the fluid looks like a heterogeneous distribution of cages, because one is not observing it in a slow enough time scale to see it relax.

V. CONCLUSION

Our 250 GHz ESR study, supplemented with 9.5 GHz results, provides detailed insights into the localized dynamics of probe molecules in OTP solvent above T_c . We find that the 250 GHz spectra of the larger CSL and MOTA probes below T_m are very well described by the dynamic cage model of Polimeno and Freed.³² The probe reorientation rates and the cage relaxation rate both follow simple Arrhenius Laws consistent with elementary rate processes. The molecular (i.e., spin independent) correlation functions for this model are themselves substantially different from simple exponential (i.e., non-Debye-like). These results are consistent with homogeneous liquidlike behavior of OTP above T_c . Attempts to reinterpret these spectra in terms of models of heterogeneous but simple (Brownian) reorientation lead to unsatisfactory fits and/or are inconsistent with the approximate Stokes-Einstein behavior found for molecular relaxation by other techniques when average reorientation (or other) rates are considered. However, the average reorientation rates obtained from the very good fits of the dynamic cage model to the ESR spectra are in accord with the results from other techniques.

In the context of the frustration-limited cluster size model of Kivelson and co-workers,¹⁷ we find that the dynamic cage, formed from the neighboring OTP molecules, reaches a certain size, on the order of 10 molecules, before the dynamics show significant departures from simple Brownian relaxation. The ESR spectra indicate the existence of substantial voids in the system which permit unhindered rotational dynamics of the small PDT molecule down to below T_m , PDT aggregation below T_c , and the existence of slow and fast components in the MOTA spectra below T_c .

The cage potential parameters for CSL and MOTA yield estimates of the orientational distribution of these probes in the cage potential. Our interpretation of these parameters suggests that, in the range of $T_m \geq T \geq T_c$, OTP packs locally like a discotic with mesogen units having the shape of a nautilus shell.

ACKNOWLEDGMENTS

We dedicate this paper to the memory of Yakov S. Lebedev. This work was supported by NSF Grant CHE9313167 and by NIH Grants RR07126 and GM25862. One of us (J.K.M.) was also partially supported by the Polish State Committee for Scientific Research (KBN) Grant No. 2 P03B 210 08 and EC Human Capital and Mobility Network Contract No. ERBCIPDCT940607. We are indebted to Professor E. W. Fischer and Dr. W. Steffen for providing us with their original FPI data, and to D. Schneider for many valuable comments and discussions. The computations reported here were performed at the Cornell Theory Center.

- ¹E. Jenckel, *Z. Phys. Chem.* **184**, 309 (1939).
- ²G. Adam and J. H. Gibbs, *J. Chem. Phys.* **43**, 139 (1965).
- ³E. Donth, *J. Non-Cryst. Solids* **53**, 325 (1982).
- ⁴C. T. Moynian and J. Schröder, *J. Non-Cryst. Solids* **160**, 52 (1993).
- ⁵M. H. Cohen and D. Turnbull, *J. Chem. Phys.* **31**, 1164 (1959).
- ⁶G. S. Grest and M. H. Cohen, in *Advances in Chemical Physics*, edited by I. Prigogine and S. A. Rice (Wiley, New York, 1981), Vol. 48, p. 455.
- ⁷E. McLaughlin and A. R. Ubbelohde, *Trans. Faraday Soc.* **54**, 1804 (1958).
- ⁸F. H. Stillinger, *J. Chem. Phys.* **89**, 6461 (1988).
- ⁹T. R. Kirkpatrick, D. Thirumalai, and P. G. Wolynes, *Phys. Rev. A* **40**, 1045 (1989).
- ¹⁰F. Fujara, B. Geil, H. Sillescu, and G. Fleischer, *Z. Phys. B* **88**, 195 (1992).
- ¹¹F. R. Blackburn, M. T. Cicerone, G. Hieptas, P. A. Wagner, and M. D. Ediger, *J. Non-Cryst. Solids* **172–174**, 256 (1994).
- ¹²M. H. Cohen and G. S. Grest, *Phys. Rev. B* **24**, 4091 (1981).
- ¹³J. A. Hodgdon and F. H. Stillinger, *Phys. Rev. E* **48**, 207 (1993).
- ¹⁴F. H. Stillinger, and J. A. Hodgdon, *Phys. Rev. E* **50**, 2064 (1994).
- ¹⁵H. Sillescu, *Phys. Rev. E* **53**, 2992 (1996).
- ¹⁶F. H. Stillinger and J. A. Hodgdon, *Phys. Rev. E* **53**, 2995 (1996).
- ¹⁷D. Kivelson, S. A. Kivelson, X. Zhao, Z. Nussinov, and G. Tarjus, *Physica A* **219**, 27 (1995).
- ¹⁸D. Kivelson, G. Tarjus, X. Zhao, and S. A. Kivelson, *Phys. Rev. E* **53**, 751 (1996).
- ¹⁹E. Leutheusser, *Phys. Rev. A* **29**, 2765 (1984).
- ²⁰U. Bengtzelius, W. Götze, and A. Sjölander, *J. Phys. C* **17**, 5915 (1984).
- ²¹W. Götze and L. Sjögren, *Rep. Prog. Phys.* **55**, 241 (1992).
- ²²W. Götze and L. Sjögren, *Transp. Theo. Stat. Phys.* **24**, 801 (1995).
- ²³E. Rössler and W. Schnauss, *Chem. Phys. Lett.* **170**, 315 (1990).
- ²⁴W. van Meegen and S. M. Underwood, *Phys. Rev. E* **47**, 248 (1993).
- ²⁵H. Z. Cummins, W. M. Du, M. Fuchs, W. Götze, S. Hildebrand, A. Latz, G. Li, and N. J. Tao, *Phys. Rev. E* **47**, 4223 (1993).
- ²⁶E. Bartsch, F. Fujara, J. F. Legrand, W. Petry, H. Sillescu, and J. Wuttke, *Phys. Rev. E* **52**, 738 (1995).
- ²⁷W. Steffen, A. Patkowski, H. Gläser, G. Meier, and E. W. Fischer, *Phys. Rev. E* **49**, 2992 (1994).
- ²⁸A. P. Sokolov, *Science* **273**, 1675 (1996).
- ²⁹K. A. Earle, D. E. Budil, and J. H. Freed, *J. Phys. Chem.* **97**, 13289 (1993).
- ³⁰D. J. Schneider and J. H. Freed, *Adv. Chem. Phys.* **73**, 387 (1989).
- ³¹J. H. Freed, in *Lecture Notes in Physics 293: Rotational Dynamics of Small and Macro-molecules*, edited by T. F. Dörfmüller and R. Pecora (Plenum, New York, 1987), p. 89.
- ³²A. Polimeno and J. H. Freed, *J. Phys. Chem.* **99**, 10995 (1995).
- ³³V. S. S. Sastry, A. Polimeno, R. H. Crepeau, and J. H. Freed, *J. Chem. Phys.* **105**, 5753 (1996); **105**, 5773 (1996).
- ³⁴S. R. Kudchadkar and J. M. Wiest, *J. Chem. Phys.* **103**, 8566 (1995).
- ³⁵M. T. Cicerone, F. R. Blackburn, and M. D. Ediger, *J. Chem. Phys.* **102**, 471 (1994).
- ³⁶M. T. Cicerone and M. D. Ediger, *J. Chem. Phys.* **97**, 2156 (1992).
- ³⁷W. Schnauss, F. Fujara, and H. Sillescu, *J. Chem. Phys.* **97**, 1378 (1992).
- ³⁸D. Kivelson, M. Greenfield, and S. Gomperts, *J. Non-Cryst. Solids* **133**, 327 (1991).
- ³⁹Aldrich Chemicals, 1994, catalogue.
- ⁴⁰C. A. Angell, in *Proceedings of the Workshop on Relaxation Effects in Disordered Systems*, edited by K. Ngai and T. K. Lee (McGregor and Werner, Blacksburg, TN, 1983), p. 3.
- ⁴¹W. C. Ehrhardt and W. E. Vaughan, *J. Chem. Phys.* **74**, 5479 (1981).
- ⁴²M. T. Cicerone and M. D. Ediger, *J. Phys. Chem.* **97**, 10489 (1993).
- ⁴³I. Chang, F. Fujara, B. Geil, G. Heuberger, T. Mangel, and H. Sillescu, *J. Non-Cryst. Solids* **172–174**, 248 (1994).
- ⁴⁴C. P. Slichter, *Principles of Magnetic Resonance* (Springer, New York, 1990), Chap. 11.
- ⁴⁵K. A. Earle, D. E. Budil, and J. H. Freed, in *Advances in Magnetic and Optical Resonance*, edited by W. Warren (Academic, New York, 1996), Vol. 19, p. 253.
- ⁴⁶W. B. Lynch, K. A. Earle, and J. H. Freed, *Rev. Sci. Instrum.* **59**, 1345 (1988).
- ⁴⁷A. Nayeem, S. B. Rananavare, V. S. S. Sastry, and J. H. Freed, *J. Chem. Phys.* **96**, 3912 (1992).
- ⁴⁸D. E. Budil, K. A. Earle, and J. H. Freed, *J. Phys. Chem.* **97**, 1294 (1993).
- ⁴⁹J. S. Hwang, R. P. Mason, L. P. Hwang, and J. H. Freed, *J. Phys. Chem.* **79**, 489 (1975).
- ⁵⁰R. J. Greet and D. Turnbull, *J. Chem. Phys.* **46**, 1243 (1966).
- ⁵¹Cf. Fig. 6(c).
- ⁵²A. Nayeem and J. H. Freed, *J. Phys. Chem.* **93**, 6539 (1989).
- ⁵³S. A. Zager and J. H. Freed, *J. Chem. Phys.* **77**, 3344 (1982).
- ⁵⁴S. A. Zager and J. H. Freed, *J. Chem. Phys.* **77**, 3360 (1982).
- ⁵⁵D. E. Budil, S. Lee, S. Saxena, and J. H. Freed, *J. Magn. Reson. A* **120**, 155 (1996).
- ⁵⁶We have independently verified by a separate rigid limit simulation that the use of the slow-motional tumbling programs is valid for extracting the rigid limit parameters. We point out that this is further evidence of the limited resolution of cw spectra to dynamics very close to the rigid limit.
- ⁵⁷A. Nayeem, S. B. Rananavare, V. S. S. Sastry, and J. H. Freed, *J. Chem. Phys.* **91**, 6887 (1989).
- ⁵⁸The rhombic component of the diffusion tensor ρ_{xy} was not varied. Its effect is small and it does not improve the quality of the fits significantly.
- ⁵⁹We found from the nonlinear least-square fits that the least reliably determined parameter was N , which tended to correlate strongly with the potential coefficients c_0^2 and c_2^2 . We have seen evidence for the effects of non-Brownian motion on the observed value of N in previous work, (Refs. 29 and 32) and we postulate that a similar effect is occurring here.
- ⁶⁰Y. Higashigaki and C. H. Wang, *J. Chem. Phys.* **74**, 3175 (1981).
- ⁶¹C. H. Wang, X. R. Zhu, and J. C. Shen, *Mol. Phys.* **62**, 749 (1987).
- ⁶²T. Dries, F. Fujara, M. Kiebel, E. Rössler, and H. Sillescu, *J. Chem. Phys.* **88**, 2139 (1988).
- ⁶³F. Fujara, *J. Mol. Struct.* **296**, 285 (1993).
- ⁶⁴G. P. Johari and M. Goldstein, *J. Chem. Phys.* **53**, 2372 (1970).
- ⁶⁵W. Steffen, A. Patkowski, G. Meier, and E. W. Fischer, *J. Chem. Phys.* **96**, 4171 (1992).
- ⁶⁶A. Patkowski, W. Steffen, G. Meier, and E. W. Fisher, *J. Non-Cryst. Solids* **172**, 52 (1994).
- ⁶⁷P. D. Hyde, T. E. Evert, and M. D. Ediger, *J. Chem. Phys.* **93**, 2274 (1990).
- ⁶⁸E. W. Montrell and J. T. Bendler, *J. Stat. Phys.* **34**, 129 (1984).
- ⁶⁹M. Abramowitz and I. A. Stegun, *Handbook of Mathematical Functions* (Dover, New York, 1965).
- ⁷⁰A. Polimeno and J. H. Freed, *Chem. Phys. Lett.* **174**, 338 (1990).
- ⁷¹A. Polimeno and J. H. Freed, *Adv. Chem. Phys.* **83**, 89 (1993).
- ⁷²D. J. Schneider, and J. H. Freed, in *Biological Magnetic Resonance*, edited by L. Berliner (Plenum, New York, 1989), Vol. 8, p. 1.
- ⁷³W. Schnauss, F. Fujara, K. Hartmann, and H. Sillescu, *Chem. Phys. Lett.* **166**, 381 (1990).
- ⁷⁴K. Schmidt-Rohr, and H. W. Spiess, *Phys. Rev. Lett.* **66**, 3020 (1991).
- ⁷⁵We can rewrite the integral equation that defines $\rho(\tau, \tau_0; \beta)$, Eq. (5), as a Laplace transform in the variables $\sigma \equiv \tau/\tau_0$ and $t' = t/\tau_0$. One may verify by inspection that $\rho(\tau, \tau_0; 1)$ is a delta function. For $\beta \neq 1$, we may use results from the theory of stable one-dimensional distributions—cf. V. M. Zolotarev “One-dimensional Stable Distributions” Transl. by B. Silver from “Odnomernye ustojchivye raspredeleniia”, ((Nauka)), Moskva, 1983, (Am. Math. Soc., Providence, Rhode Island, 1986)—to write $\rho(\tau, \tau_0; \beta)$ in terms of stable one-dimensional distributions. Tables of stable one-dimensional distributions for various values of β may be found in, e.g., D. R. Holt and E. L. Crow, *J. Res. Natl. Bur. Stand. B* **77**, 143 (1973).
- ⁷⁶We have also considered inhomogeneous distributions over more re-

- stricted regions. We do find that if the distribution in τ/τ_0 is restricted to ~ 1 decade, then there are improvements in the fits to the experimental ESR spectra over those from simple Brownian motion, but they are not as good as those we obtain with the dynamic cage model. (In particular, the g_x region is reduced in amplitude, while the g_y region is increased in amplitude, both in a manner consistent with experiment, but the g_z region is also reduced in amplitude, and this is inconsistent with experiment.) Also, these restricted ranges of τ/τ_0 correspond to values of $\beta \approx 0.9$ which would be inconsistent with the results of other physical techniques, whereas the values of $\beta \approx 0.6$ we obtain for these ESR spectra with the dynamic cage model fits are consistent, as we have shown above.
- ⁷⁷ A. Einstein, *Ann. Phys. (Leipzig)* **19**, 371 (1906).
- ⁷⁸ P. Debye, *Polar Molecules* (Dover, New York, 1929), pp. 77–86.
- ⁷⁹ F. Perrin, *J. Phys. Radium* **7**, 1 (1936).
- ⁸⁰ L. D. Landau and E. M. Lifshitz, *Fluid Mechanics* (Pergamon, New York, 1982), pp. 227–229.
- ⁸¹ M. Lohfink and H. Sillescu, *AIP Conf. Proc.* **256**, 30 (1992).
- ⁸² D. W. McCall, D. C. Douglass, and D. R. Falcone, *J. Chem. Phys.* **50**, 3839 (1969).
- ⁸³ W. Petry, E. Batsch, F. Fujara, M. Kiebel, H. Sillescu, and B. Farago, *Z. Phys. B* **83**, 17 (1991).
- ⁸⁴ S. A. Kivelson, X. Zhao, D. Kivelson, T. M. Fischer, and C. M. Knobler, *J. Chem. Phys.* **101**, 2391 (1994).
- ⁸⁵ S. S. N. Murthy, A. Paikaray, and N. Arya, *J. Chem. Phys.* **102**, 8213 (1995).
- ⁸⁶ L. J. Lewis and G. Wahnström, *Phys. Rev. E* **50**, 3865 (1994).
- ⁸⁷ S. Matsuoka and X. Quan, *J. Non-Cryst. Solids* **131**, 293 (1991).
- ⁸⁸ Our dynamic cage model (Ref. 32) is based on cage relaxation as a result of its reorientation due to solvent redistribution. For simplicity we have neglected a distribution in the magnitude of the potential coefficients e.g., c_0^2 and c_2^2 of Eq. (1). Molecular dynamics calculations on the dynamic cage for a simple fluid (liquid Cl_2) do show that a modest distribution in the magnitude of the cage potential is present, but the rate of fluctuations in magnitude is slower than its reorientational relaxation [A. Polimeno, G. J. Moro, and J. H. Freed, *J. Chem. Phys.* **102**, 9094 (1995); **104**, 1090 (1996)]. We do not know whether this would also be true for OTP.
- ⁸⁹ We would like to emphasize that the spectra that we see below T_c are actually of the two-component type. Given the simulation of Fig. 12, and the discussion in Sec. IV B, one might be inclined to suggest the possibility of a distribution of relaxation times. The distinctive feature of Fig. 12 is the presence of a well-resolved motionally-narrowed component, despite the distribution, which arises precisely because of the sharpness (i.e., narrowness) of the hf components. Instead, the more rapidly tumbling component in the MOTA spectra below T_c is characteristic of the incipient smr, which is actually quite broad. A restricted distribution, covering the incipient smr to deep into the smr would still be a broad superposition and not have the distinctive two-component features seen experimentally, [cf. Fig. 1(b)].
- ⁹⁰ K. A. Earle, J. K. Moscicki, A. Polimeno, and J. H. Freed (in preparation).